IN THE UNITED STATES PATENT AND TRADEMARK OFFICE

Applicant:	MOECKLY	Examiner:	P. WARTALOWICZ
Serial No.:	10/751,091	Group Art Unit:	1793
Filed:	JANUARY 2, 2004	Docket No.:	10467.43USI2
Title:	HIGH-TEMPERATURE SUPERCONDUCTOR DEVICES AND METHODS OF FORMING THE SAME		

Electronically filed on April 14, 2010.

APPELLANT'S BRIEF ON APPEAL

Commissioner for Patents
P.O. Box 1450
Alexandria, Virginia 22313-1450

Sir:

This Brief is presented in support of the Appeal filed 14 January 2010, from the rejection of Claims 65-68 and 71-75 of the above-identified application, as set forth in the Office Action mailed on 14 October 2009 ("Appealed Office Action").

It is believed that the previously paid appeal brief fee of $270 should be applied to, and is sufficient to cover the required fee for, the filing of this Brief. *See*, MPEP at 1207.04. Please charge any additional fees required or credit any overpayment to Deposit Account. No. 13-2725.

An oral hearing is requested. A separate request for oral hearing with the appropriate fee will be filed within two months of the Examiner's Answer.

I. REAL PARTY OF INTEREST

The real party in interest is the Superconductor Technologies Inc. of Santa Barbara, California.

II. RELATED APPEALS AND INTERFERENCES

None.

III. STATUS OF CLAIMS

Claims 65-68 and 71-75 are pending and stand rejected. Claims 1-64 and 69-70 have been cancelled. Claims 65-68 and 71-75 are on appeal and are listed in the CLAIMS APPENDIX.

IV. STATUS OF AMENDMENTS

No amendment has been made since the Office Action of 14 October 2009.

V. SUMMARY OF THE CLAIMED SUBJECT MATTER

In the following summary, Appellants provide exemplary references to sections of the specification and/or drawings supporting the subject matter as defined in the claims as required by 37 C.F.R. § 41.37(c)(1)(v). The specification and drawings also include additional support for other exemplary embodiments encompassed by the claimed subject matter. Thus, it should be appreciated that the references are not exhaustive and are intended only to be illustrative in nature.

A. Independent Claim 65

Appellants note that the language of claim 65 defines the scope of the subject matter of the claim. The summary below is intended for the convenience of the Board and is not intended to limit the scope of the claim.

Claim 65 recites a Josephson junction device. *See, e.g.,* Figure 1; p. 7, lines 11-14; . The Josephson junction is one of the basic elements of superconductor electronic devices, and is well-developed in low temperature superconductors. *See, e.g.,* p. 3, line 14-15. The invention claimed in the claim 65 relates to a Josephson junction device using high-temperature superconductors. The device comprises:

a first layer comprising an oxide high-temperature superconductor (*e.g.,* the layer reference labeled "12" in Figure 1; p. 10, lines 23-27);

a second layer comprising an oxide high-temperature superconductor (*e.g.,* the layer reference labeled "18" in Figure 1; p. 11, lines 5-7; p. 12, lines 13-14); and

a third layer (*e.g.,* the layer reference labeled "20" in Figure 1) connecting the first and second layers and comprising a non-superconductor,

the first and third layers being formed from a starting oxide high-temperature superconductor layer of an oxide high-temperature superconductor, the third layer being an ion-modified portion of the starting oxide high-temperature superconductor layer, the first layer being an unmodified portion of the starting oxide high-temperature superconductor layer (p. 11, line 21-23 (the exposed surface layer 20 of the high-temperature superconductor layer is converted to a layer of a difference phase, structure or chemical composition.)),

the device having an R_nA value of about 1×10^{-9} to about 3×10^{-7} Ω-cm^2 at 4.2 K (*see, e.g.*, Figure 6 and p. 13, lines 5-9).

It should be noted that support for claim 65 also lies in other portions of the written description as well as in other figures. For clarity, Appellant only cites to the above portions of the specification and figures.

B. Independent Claim 67

Appellants note that the language of claim 67 defines the scope of the subject matter of the claim. The summary below is intended for the convenience of the Board and is not intended to limit the scope of the claim.

Claim 67 recites an electronic device comprising:

a crystalline substrate (Ref. 10 in Figure 1; p. 10, line 9-16);

an electrode formed on and epitaxial to the substrate, the electrode comprising a first superconductive oxide (e.g., the layer reference labeled "12" in Figure 1; p. 10, line 23-p. 11, line 27);

a barrier comprising a non-superconducting, ion-modified surface layer of the first superconductive oxide (e.g., the layer reference labeled "20" in Figure 1; p. 11, line 21-23 (the exposed surface layer 20 of the high-temperature superconductor layer is converted to a layer of a difference phase, structure or chemical composition.)); and

a counter-electrode formed directly on and epitaxial to the barrier, the counter-electrode comprising a second superconductive oxide (*e.g.*, the layer reference labeled "18" in Figure 1; p. 11, lines 5-7; p. 12, lines 13-14; p. 7, lines 15-20; original claim 1), whereby a Josephson junction is formed between the electrode and the counter-electrode, having an R_nA value of about 1×10^{-9} to about 3×10^{-7} Ω-cm^2 at 4.2 K (*see, e.g.*, Figure 6 and p. 13, lines 5-9).

It should be noted that support for claim 67 also lies in other portions of the written description as well as in other figures. For clarity, Appellant cites only to the above portions of the specification and figures.

C. Independent Claim 71

Appellants note that the language of claim 71 defines the scope of the subject matter of the claim. The summary below is intended for the convenience of the Board and is not intended to limit the scope of the claim.

Claim 71 recites a Josephson junction device. *See, e.g.*, Figure 1; p. 7, lines 11-14; . The Josephson junction is one of the basic elements of superconductor electronic devices, and is well-developed in low temperature superconductors. *See, e.g.*, p. 3, line 14-15. The invention claimed in the claim 65 relates to a Josephson junction device using high-temperature superconductors. The device comprises:

a first layer comprising an oxide high-temperature superconductor (*e.g.*, the layer reference labeled "12" in Figure 1; p. 10, lines 23-27);

a second layer comprising an oxide high-temperature superconductor (*e.g.*, the layer reference labeled "18" in Figure 1; p. 11, lines 5-7; p. 12, lines 13-14); and

a third layer (*e.g.*, the layer reference labeled "20" in Figure 1) connecting the first and second layers and comprising a non-superconductor,

the first and third layers being formed from a starting oxide high-temperature superconductor layer of an oxide high-temperature superconductor, the third layer being an ion-modified portion of the starting oxide high-temperature superconductor layer, the first layer being an unmodified portion of the starting oxide high-temperature superconductor layer (p. 11, line 21-23 (the exposed surface layer 20 of the high-temperature superconductor layer is converted to a layer of a difference phase, structure or chemical composition.)),

the device having a J_c value of about 1×10^3 to about 5×10^6 A/cm^2 at 4.2 K. (*See, e.g.*, Figure 6 and p. 13, line 5-19.)

It should be noted that support for claim 71 also lies in other portions of the written description as well as in other figures. For clarity, Appellant only cites to the above portions of the specification and figures.

D. Independent Claim 73

Appellants note that the language of claim 73 defines the scope of the subject matter of the claim. The summary below is intended for the convenience of the Board and is not intended to limit the scope of the claim.

Claim 73 recites an electronic device comprising:

a crystalline substrate (Ref. 10 in Figure 1; p. 10, line 9-16);

an electrode formed on and epitaxial to the substrate, the electrode comprising a first superconductive oxide (e.g., the layer reference labeled "12" in Figure 1; p. 10, line 23-p. 11, line 27);

a barrier comprising a non-superconducting, ion-modified surface layer of the first superconductive oxide (e.g., the layer reference labeled "20" in Figure 1; p. 11, line 21-23 (the exposed surface layer 20 of the high-temperature superconductor layer is converted to a layer of a difference phase, structure or chemical composition.)); and

a counter-electrode formed directly on and epitaxial to the barrier, the counter-electrode comprising a second superconductive oxide (e.g., the layer reference labeled "18" in Figure 1; p. 11, lines 5-7; p. 12, lines 13-14; p. 7, lines 15-20; original claim 1), whereby a Josephson junction is formed between the electrode and the counter-electrode,

the device having a J_c value of about 1×10^3 to about 5×10^6 A/cm^2 at 4.2 K (*See, e.g.*, Figure 6 and p. 13, line 5-19.).

It should be noted that support for claim 73 also lies in other portions of the written description as well as in other figures. For clarity, Appellant cites only to the above portions of the specification and figures.

VI. GROUNDS OF REJECTION TO BE REVIEWED ON APPEAL

Claims 71-74 stand rejected under 35 U.S.C. § 112, ¶ 1, as failing to comply with the written-description requirement. Specifically, the Examiner takes the position that the recited critical current density range is not supported by the Specificaiton. Appealed Office Action at p. 2.

Claims 65-68 and 71-75 stand rejected under 35 U.S.C. 102(b) as anticipated by or, in the alternative, under 35 U.S.C. 103(a) as obvious over B.D. Hunt *et al.*, "All high Tc edge-geometry weak links utilizing Y-Ba-Cu-O barrier layers", *Appl. Phys. Lett.* 59 (8), pp. 982-984 (19 August 1991) ("Hunt 1991 Article"). Appealed Office Action at pp. 3-4.

Claims 65-68, 71-75 stand rejected also under 35 U.S.C. 102(e) as anticipated by or, in the alternative, under 35 U.S.C. 103(a) as obvious over U.S. Patent No 5,945,383 (to Brian D. Hunt) ("Hunt Patent"). Appealed Office Action at p. 5.

VII. ARGUMENT

Claim Rejection – 35 U.S.C. § 112, ¶1

In rejecting Claims 71-74, the Examiner states that it is unclear that the recitation in claims 71 and 73 of a critical current density (J_c) of about 1×10^3 to about 5×10^6 A/cm^2 at 4.2 K has support in the specification. Appealed Office Action at p. 2. The Examiner further cites Figure 6 in the Specification as supporting a critical current density range of about 2.0×10^3 to about 4.0×10^6 A/cm^2. *Id.*

In response, Applicants respectfully draw the Board's attention to not only Figure 6 but also the Specification at p. 13, lines 5-7: "In Figure 6, the ranges of I_cR_n and R_n that are attainable at 4.2 K are displayed. Note that I_cR_n products from 0.3 to 5 mV are possible, with ***corresponding*** R_nA values of 3×10^{-7} to 1×10^{-9} Ωcm^2." (emphasis added.) The various symbols are defined at p. 3, lines 18-20: "[Josephson junctions] are characterized by a critical current density J_c, a critical current I_c, an effective device cross-sectional area A, junction resistance, R_n, and normalized junction resistance R_nA." As the I_cR_n products correspond to R_nA, the ratio between the two is clearly the critical current divided by the cross-sectional area, *i.e.*, the critical current density. Applicants therefore respectfully submit that the recited critical current density range is adequately supported by the Specification.

For at least these reasons, Applicants respectfully request that the Examiner's rejection under 35 U.S.C. § 112, ¶1 be reversed.

Claim Rejection – 35 U.S.C. § 102 or 103

As to the rejections for anticipation under 35 U.S.C. § 102, a claim is anticipated "only if each and every element as set forth in the claim is found, either expressly or inherently described, in a single prior art reference." *MPEP* 2131 (citing *Verdegaal Bros. v. Union Oil Co. of California*, 814 F.2d 628, 631, 2 USPQ2d 1051, 1053 (Fed. Cir. 1987)). As to the rejections for obviousness under 35 U.S.C. § 103, "[r]ejections on obviousness grounds cannot be sustained by mere conclusory statements; instead, there must be some articulated reasoning with some rational underpinning to support the legal conclusion of obviousness." *KSR Int'l Co. v. Teleflex Inc.*, 127 S. Ct. 1727, 1741 (2007). To establish a *prima facie* case of obviousness under 35 U.S.C. § 103(a), the references must teach or suggest all of the claimed limitations to one of ordinary skill in the art at the time the invention was made. *In re Royka*, 490 F.2d 981, 985

(C.C.P.A. 1974); *In re Wilson*, 424 F.2d 1382, 1385 (C.C.P.A. 1970); *Ex Parte Wada and Murphy*, BPAI Appeal No. 2007-3733 (January 14, 2008) (quoting *In re Ochiai*, 71 F.3d 1565, 1572 (Fed. Cir. 1995) and *CFMT, Inc. v. Yieldup Intern. Corp.*, 349 F.3d 1333, 1342 (Fed. Cir. 2003)). *See also*, M.P.E.P § 2143.03 ("All claim limitations must be considered.") Appellants submit that the Examiner has failed to demonstrate anticipation or state a *prima facie* case for obviousness in rejecting the independent claims.

Each of independent Claims 65 and 71includes, among other things, the feature of "the ***third layer being an ion-modified portion of the starting oxide high-temperature superconductor layer***, the first layer being an unmodified portion of the starting oxide high-temperature superconductor layer." (Emphasis added.) Each of independent Claims 67 and 73 includes, among other things, the feature of "a barrier comprising a non-superconducting, ***ion-modified surface layer of the first superconductive oxide***." (Emphasis added.) As the above-cited features are process features, the claims are product-by-process claims, as acknowledged by the Examiner. Appealed Office Action at pp. 4 and 5.

In its most recent *en banc* decision on the scope of product-by-process claims, the U.S. Court of Appeals for the Federal Circuit has held that product-by-process claims are limited by the process recited in the claims. *Abbott Laboratories v. Sandoz, Inc.*, 566 F.3d 1282, 1291(Fed. Cir. 2009) (*en banc*). While the *Abbott* Court's focus is on infringement analysis, it is well-established that patent claims are construed the same way for validity and for infringement. *See, e.g.*, *Amgen Inc. v. Hoechst Marion Roussel, Inc.*, 314 F.3d 1313, 1330 (Fed. Cir. 2003) ("It is axiomatic that claims are construed the same way for both invalidity and infringement."); *Amazon.com, Inc. v. Barnesandnoble.com, Inc.*, 239 F.3d 1343, 1351 (Fed. Cir. 2001) ("Because the claims of a patent measure the invention at issue, the claims must be interpreted and given the same meaning for purposes of both validity and infringement analyses.") Thus, the scopes of the independent claims, and thus all pending claims, are limited by the above-cited process features.

The Hunt 1991 Article and Hunt Patent both fail to disclose or suggest the process features of the rejected claims. To the contrary, both references teaches away from forming barrier by ion-modification according to the claimed invention by teaching a ***deposited*** barrier layer. *See, e.g.*, Hunt 1991 Article at p. 982; Hunt Patent at Abstract and col. 5, line 54-col. 6,

line 32. The Examiner also has not articulated any reason how the process features could have been obvious in light of the references.

Furthermore, the Examiner has not established that the ion-modified barrier recited in the rejected claims and deposited barrier disclosed in the Hunt references are "substantially identical". *See, MPEP* 2113. As is conceded in the Hunt 1991 Article at p. 983, the non-superconducting barrier had not been extensively characterized, and that the oxygen stoichiometry and structure of the deposited barrier was "not known." *See, also,* Hunt Patent at col. 5, lines 27-40. As discussed in another article ("Hunt 1993 Article") authored by B.D. Hunt *et al.* subsequent to the publication of the Hunt 1991 Article, there are numerous possible phases of the non-superconducting barrier. *Id.* at p. 4. There is therefore not a reasonable basis to assert that the barriers of the claimed product and product disclosed in the Hunt 1991 Article or Hunt Patent are substantially identical.

Therefore, Applicants respectfully submit that the appealed claims are not obvious over either the Hunt 1991 Article or Hunt Patent.

SUMMARY

Applicants therefore respectfully request that the Examiner's rejection be reversed, and that all of the pending claims be allowed.

Respectfully submitted,

MERCHANT & GOULD P.C.
P.O. Box 2903
Minneapolis, Minnesota 55402-0903
(612) 332-5300

Date: 14 April 2010

/Tong Wu/
Tong Wu
Reg. No. 43,361
TW:cjc

CLAIMS APPENDIX

65. A Josephson junction device, comprising:

a first layer comprising an oxide high-temperature superconductor;

a second layer comprising an oxide high-temperature superconductor; and

a third layer connecting the first and second layers and comprising a non-superconductor,

the first and third layers being formed from a starting oxide high-temperature superconductor layer of an oxide high-temperature superconductor, the third layer being an ion-modified portion of the starting oxide high-temperature superconductor layer, the first layer being an unmodified portion of the starting oxide high-temperature superconductor layer,

the device having an R_nA value of about 1×10^{-9} to about 3×10^{-7} Ω-cm^2 at 4.2 K.

66. The Josephson junction device of claim 65, wherein the first layer comprises an YBCO superconducting oxide.

67. An electronic device comprising:

a crystalline substrate;

an electrode formed on and epitaxial to the substrate, the electrode comprising a first superconductive oxide;

a barrier comprising a non-superconducting, ion-modified surface layer of the first superconductive oxide; and

a counter-electrode formed directly on and epitaxial to the barrier, the counter-electrode comprising a second superconductive oxide, whereby a Josephson junction is formed between the electrode and the counter-electrode, having an R_nA value of about 1×10^{-9} to about 3×10^{-7} Ω-cm^2 at 4.2 K.

68. The device of claim 67, wherein the first and second superconductive oxides are YBCO.

71. A Josephson junction device, comprising:

a first layer comprising an oxide high-temperature superconductor;

a second layer comprising an oxide high-temperature superconductor; and

a third layer connecting the first and second layers and comprising a non-superconductor,

the first and third layers being formed from a starting oxide high-temperature superconductor layer of an oxide high-temperature superconductor, the third layer being an ion-modified portion of the starting oxide high-temperature superconductor layer, the first layer being an unmodified portion of the starting oxide high-temperature superconductor layer,

the device having a J_c value of about 1×10^3 to about 5×10^6 A/cm^2 at 4.2 K.

72. The Josephson junction device of claim 71 wherein the first layer comprises an YBCO superconducting oxide.

73. An electronic device comprising:

a crystalline substrate;

an electrode formed on and epitaxial to the substrate, the electrode comprising a first superconductive oxide;

a barrier comprising a non-superconducting, ion-modified surface layer of the first superconductive oxide; and

a counter-electrode formed directly on and epitaxial to the barrier, the counter-electrode comprising a second superconductive oxide, whereby a Josephson junction is formed between the electrode and the counter-electrode,

the device having a J_c value of about 1×10^3 to about 5×10^6 A/cm^2 at 4.2 K.

74. The Josephson junction device of claim 73, wherein the first and second superconductive oxides are YBCO.

75. The Josephson junction device of claim 65, wherein the third layer is substantially uniform.

EVIDENCE APPENDIX

A. OFFICE ACTIONS AND AMENDMENTS/RESPONSES

1. Office Action -- mailed 14 October 2009

B. REFERENCES RELIED UPON BY THE EXAMINER

1. B.D. Hunt *et al.*, "All high Tc edge-geometry weak links utilizing Y-Ba-Cu-O barrier layers", *Appl. Phys. Lett.* 59 (8), pp. 982-984 (19 August 1991)
2. U.S. Patent No. 5,945,383
3. Hunt, B. *et al.*, "High Temperature Superconductor Weak Links", *Second Symposium on Low Temperature Electronics and High Temperature Superconductivity,* Electrochemical Society Meeting, Honolulu, Hawaii, Vol. 93-22, p. 467-472 (May 1993)

RELATED PROCEEDINGS APPENDIX

None.

USSN 10/751,091

EVIDENCE APPENDIX

ATTACHMENT A.1

UNITED STATES PATENT AND TRADEMARK OFFICE

UNITED STATES DEPARTMENT OF COMMERCE
United States Patent and Trademark Office
Address: COMMISSIONER FOR PATENTS
P.O. Box 1450
Alexandria, Virginia 22313-1450
www.uspto.gov

APPLICATION NO.	FILING DATE	FIRST NAMED INVENTOR	ATTORNEY DOCKET NO.	CONFIRMATION NO.
10/751,091	01/02/2004	Brian H. Moeckly	10467.43US12	2150

23552 7590 10/14/2009

MERCHANT & GOULD PC
P.O. BOX 2903
MINNEAPOLIS, MN 55402-0903

EXAMINER	
WARTALOWICZ, PAUL A	
ART UNIT	PAPER NUMBER
1793	

MAIL DATE	DELIVERY MODE
10/14/2009	PAPER

Please find below and/or attached an Office communication concerning this application or proceeding.

The time period for reply, if any, is set in the attached communication.

Office Action Summary	Application No.	Applicant(s)	
	10/751,091	MOECKLY ET AL.	
	Examiner	Art Unit	
	PAUL A. WARTALOWICZ	1793	

-- The MAILING DATE of this communication appears on the cover sheet with the correspondence address --

Period for Reply

A SHORTENED STATUTORY PERIOD FOR REPLY IS SET TO EXPIRE 3 MONTH(S) OR THIRTY (30) DAYS, WHICHEVER IS LONGER, FROM THE MAILING DATE OF THIS COMMUNICATION.

- Extensions of time may be available under the provisions of 37 CFR 1.136(a). In no event, however, may a reply be timely filed after SIX (6) MONTHS from the mailing date of this communication.
- If NO period for reply is specified above, the maximum statutory period will apply and will expire SIX (6) MONTHS from the mailing date of this communication.
- Failure to reply within the set or extended period for reply will, by statute, cause the application to become ABANDONED (35 U.S.C. § 133). Any reply received by the Office later than three months after the mailing date of this communication, even if timely filed, may reduce any earned patent term adjustment. See 37 CFR 1.704(b).

Status

1)☒ Responsive to communication(s) filed on *01 May 2009*.

2a)☐ This action is **FINAL**. 2b)☒ This action is non-final.

3)☐ Since this application is in condition for allowance except for formal matters, prosecution as to the merits is closed in accordance with the practice under *Ex parte Quayle*, 1935 C.D. 11, 453 O.G. 213.

Disposition of Claims

4)☒ Claim(s) *65-68 and 71-75* is/are pending in the application.

4a) Of the above claim(s) _____ is/are withdrawn from consideration.

5)☐ Claim(s) _____ is/are allowed.

6)☒ Claim(s) *65-68 and 71-75* is/are rejected.

7)☐ Claim(s) _____ is/are objected to.

8)☐ Claim(s) _____ are subject to restriction and/or election requirement.

Application Papers

9)☐ The specification is objected to by the Examiner.

10)☐ The drawing(s) filed on _____ is/are: a)☐ accepted or b)☐ objected to by the Examiner.

Applicant may not request that any objection to the drawing(s) be held in abeyance. See 37 CFR 1.85(a).

Replacement drawing sheet(s) including the correction is required if the drawing(s) is objected to. See 37 CFR 1.121(d).

11)☐ The oath or declaration is objected to by the Examiner. Note the attached Office Action or form PTO-152.

Priority under 35 U.S.C. § 119

12)☐ Acknowledgment is made of a claim for foreign priority under 35 U.S.C. § 119(a)-(d) or (f).

a)☐ All b)☐ Some * c)☐ None of:

1.☐ Certified copies of the priority documents have been received.

2.☐ Certified copies of the priority documents have been received in Application No. _____.

3.☐ Copies of the certified copies of the priority documents have been received in this National Stage application from the International Bureau (PCT Rule 17.2(a)).

* See the attached detailed Office action for a list of the certified copies not received.

Attachment(s)

1) ☒ Notice of References Cited (PTO-892)
2) ☐ Notice of Draftsperson's Patent Drawing Review (PTO-948)
3) ☐ Information Disclosure Statement(s) (PTO/SB/08) Paper No(s)/Mail Date _____.
4) ☐ Interview Summary (PTO-413) Paper No(s)/Mail Date. _____ .
5) ☐ Notice of Informal Patent Application
6) ☐ Other: _____.

DETAILED ACTION

Response to Arguments

Applicant's arguments with respect to claims 65-68 and 71-75 have been considered but are moot in view of the new ground(s) of rejection.

Claim Rejections - 35 USC § 112

The following is a quotation of the first paragraph of 35 U.S.C. 112:

> The specification shall contain a written description of the invention, and of the manner and process of making and using it, in such full, clear, concise, and exact terms as to enable any person skilled in the art to which it pertains, or with which it is most nearly connected, to make and use the same and shall set forth the best mode contemplated by the inventor of carrying out his invention.

Claims 71-74 are rejected under 35 U.S.C. 112, first paragraph, as failing to comply with the written description requirement. The claim(s) contains subject matter which was not described in the specification in such a way as to reasonably convey to one skilled in the relevant art that the inventor(s), at the time the application was filed, had possession of the claimed invention.

Claims 71 and 73 recite "having a Jc value of about 1 * 103 to about 5 * 106 A/cm2 at 4.2 K." However, it is unclear that this recitation has support in the specification. Applicant is requested to point out support for this recitation in the specification. Additionally, it appears that the only recitation of Jc in the specification is the graph of fig. 6. However, this graph does not appear to give support to the range of $1.0 * 10^3$ A/cm^2 to $5.0 * 10^6$ A/cm^2. Fig. 6 appears to give support for about $2.0 * 10^3$ A/cm^2 to about $4.0 * 10^6$ A/cm^2.

Clarification and/or correction is required.

Claim Rejections - 35 USC § 102/103

The following is a quotation of the appropriate paragraphs of 35 U.S.C. 102 that form the basis for the rejections under this section made in this Office action:

> A person shall be entitled to a patent unless –
>
> (b) the invention was patented or described in a printed publication in this or a foreign country or in public use or on sale in this country, more than one year prior to the date of application for patent in the United States.
> (e) the invention was described in a patent granted on an application for patent by another filed in the United States before the invention thereof by the applicant for patent, or on an international application by another who has fulfilled the requirements of paragraphs (1), (2), and (4) of section 371(c) of this title before the invention thereof by the applicant for patent.

The changes made to 35 U.S.C. 102(e) by the American Inventors Protection Act of 1999 (AIPA) and the Intellectual Property and High Technology Technical Amendments Act of 2002 do not apply when the reference is a U.S. patent resulting directly or indirectly from an international application filed before November 29, 2000. Therefore, the prior art date of the reference is determined under 35 U.S.C. 102(e) prior to the amendment by the AIPA (pre-AIPA 35 U.S.C. 102(e)).

The following is a quotation of 35 U.S.C. 103(a) which forms the basis for all obviousness rejections set forth in this Office action:

> (a) A patent may not be obtained though the invention is not identically disclosed or described as set forth in section 102 of this title, if the differences between the subject matter sought to be patented and the prior art are such that the subject matter as a whole would have been obvious at the time the invention was made to a person having ordinary skill in the art to which said subject matter pertains. Patentability shall not be negatived by the manner in which the invention was made.

The factual inquiries set forth in *Graham* **v.** *John Deere Co.*, 383 U.S. 1, 148 USPQ 459 (1966), that are applied for establishing a background for determining obviousness under 35 U.S.C. 103(a) are summarized as follows:

1. Determining the scope and contents of the prior art.
2. Ascertaining the differences between the prior art and the claims at issue.
3. Resolving the level of ordinary skill in the pertinent art.

4. Considering objective evidence present in the application indicating obviousness or nonobviousness.

Claims 65-68, 71-75 are rejected under 35 U.S.C. 102(b) as anticipated by or, in the alternative, under 35 U.S.C. 103(a) as obvious over Hunt ("All high Tc edge-geometry...").

Hunt teaches a superconductor Josephson element (pp. 982) comprising a first layer of YBCO base electrode deposited on a surface of a substrate (pp. 982-983), thereinafter a barrier layer of non-superconducting YBCO deposited on the base electrode, thereinafter a counter-electrode YBCO superconducting layer deposited on the non-superconducting barrier layer YBCO (pp. 982-983). Hunt also discloses that the Josephson junction has a J_c of $8.3 * 10^3$ A/cm^2 and a R_nA of $1.2 * 10^{-8}$ Ω-cm^2 for a barrier layer thickness of 100 Å wherein the barrier layer is uniform (pp. 982-984).

Regarding the limitation that the barrier comprises a non-superconducting, ion-modified surface layer of the first superconductive oxide, it appears that Hunt teaches a substantially similar product, i.e. a non-superconducting barrier layer formed of non-superconducting YBCO which has close lattice matching with superconducting layer of YBCO (pp. 982-984). It appears that the instantly claimed product by process is the same as that which is claimed (a non-superconducting barrier layer formed of non-superconducting YBCO which has close lattice matching with superconducting layer of YBCO). When the examiner has found a substantially similar product as in the applied prior art, the burden of proof is shifted to the applicant to establish that their product is patentably distinct and not the examiner to show the same process as making. *In re Brown*, 173 USPQ 685 and *In re Fessman*, 180 USPQ 324.

Claims 65-68, 71-75 are rejected under 35 U.S.C. 102(e) as anticipated by or, in the alternative, under 35 U.S.C. 103(a) as obvious over Hunt (US 5945383).

Hunt teaches a superconductor Josephson element (col. 3) comprising a first layer of YBCO base electrode deposited on a surface of a substrate (col. 3-4), thereinafter a barrier layer of non-superconducting YBCO deposited on the base electrode, thereinafter a counter-electrode YBCO superconducting layer deposited on the non-superconducting barrier layer YBCO (col. 3-4). Hunt also discloses that the Josephson junction has a J_c of $8.3 * 10^3$ A/cm^2 and a R_nA of $1.2 * 10^{-8}$ Ω-cm^2 for a barrier layer thickness of 100 Å wherein the barrier layer is uniform (col. 7-8).

Regarding the limitation that the barrier comprises a non-superconducting, ion-modified surface layer of the first superconductive oxide, it appears that Hunt teaches a substantially similar product, i.e. a non-superconducting barrier layer formed of non-superconducting YBCO which has close lattice matching with superconducting layer of YBCO (col. 4). It appears that the instantly claimed product by process is the same as that which is claimed (a non-superconducting barrier layer formed of non-superconducting YBCO which has close lattice matching with superconducting layer of YBCO). When the examiner has found a substantially similar product as in the applied prior art, the burden of proof is shifted to the applicant to establish that their product is patentably distinct and not the examiner to show the same process as making. *In re Brown*. 173 USPQ 685 and *In re Fessman*, 180 USPQ 324.

Conclusion

Any inquiry concerning this communication or earlier communications from the examiner should be directed to PAUL A. WARTALOWICZ whose telephone number is (571)272-5957. The examiner can normally be reached on 8:30-6 M-Th and 8:30-5 on Alternate Fridays.

If attempts to reach the examiner by telephone are unsuccessful, the examiner's supervisor, Stanley Silverman can be reached on (571) 272-1358. The fax phone number for the organization where this application or proceeding is assigned is 571-273-8300.

Information regarding the status of an application may be obtained from the Patent Application Information Retrieval (PAIR) system. Status information for published applications may be obtained from either Private PAIR or Public PAIR. Status information for unpublished applications is available through Private PAIR only. For more information about the PAIR system, see http://pair-direct.uspto.gov. Should you have questions on access to the Private PAIR system, contact the Electronic Business Center (EBC) at 866-217-9197 (toll-free). If you would like assistance from a USPTO Customer Service Representative or access to the automated information system, call 800-786-9199 (IN USA OR CANADA) or 571-272-1000.

Paul Wartalowicz
October 11, 2009

/Stanley Silverman/
Supervisory Patent Examiner, AU 1793

USSN 10/751,091

EVIDENCE APPENDIX

ATTACHMENT B.1

All high T_c edge-geometry weak links utilizing Y-Ba-Cu-O barrier layers

B. D. Hunt, M. C. Foote, and L. J. Bajuk
Jet Propulsion Laboratory, California Institute of Technology, Pasadena, California 91109

(Received 8 April 1991; accepted for publication 13 June 1991)

High quality $YBa_2Cu_3O_{7-x}$/normal-metal/$YBa_2Cu_3O_{7-x}$ edge-geometry weak links have been fabricated using nonsuperconducting Y-Ba-Cu-O barrier layers deposited by laser ablation at reduced growth temperatures. Devices incorporating 25–100 Å thick barrier layers exhibit current-voltage characteristics consistent with the resistively shunted junction model, with strong microwave and magnetic field response at temperatures up to 85 K. The critical currents vary exponentially with barrier thickness, and the resistances scale linearly with Y-Ba-Cu-O interlayer thickness and device area, indicating good barrier uniformity, with an effective normal metal coherence length of 20 Å.

All high T_c Josephson weak links are potentially useful for high-frequency sources and detectors, for high-speed, low-power digital logic, and for sensitive magnetic field detectors. For optimal performance in these applications, certain device characteristics are desirable, including large (>1 mV) values of the critical current-normal state resistance product (I_cR_n) accompanied by strong ac and dc Josephson response, device resistances on the order of 50 Ω, and high critical current densities (J_c) for high-speed operation. A great deal of effort has been focused on obtaining useful all high T_c Josephson devices with reports on a wide variety of device structures.[1–12] Although good progress has been made with these devices, their electrical characteristics are often less than ideal with many devices suffering from one or more of the following problems: (1) current-voltage (I-V) characteristics inconsistent with the resistively shunted junction (RSJ) model, (2) weak magnetic field and microwave response, and (3) low I_cR_n products (<500 μV).

In an effort to obtain improved device performance, this letter examines the use of a novel weak link barrier material: nonsuperconducting Y-Ba-Cu-O (N-YBaCuO) grown at reduced temperature. This study was motivated by the fact that oxygen-deficient $YBa_2Cu_3O_{7-x}$ exhibits a reduced or zero transition temperature,[13] and hence might be suitable for weak coupling of more completely oxidized $YBa_2Cu_3O_{7-x}$ layers. In addition, there has been a recent report of a new cubic semiconducting phase of $YBa_2Cu_3O_{7-x}$ produced by laser ablation at growth temperatures near 560 °C.[14] The use of Y-Ba-Cu-O barrier layers has the obvious advantage of chemical compatibility with the device electrodes. It is also expected that such layers should allow epitaxial overgrowth of $YBa_2Cu_3O_{7-x}$, because the lattice constants reported for oxygen-deficient $YBa_2Cu_3O_{7-x}$ and for the possible cubic $YBa_2Cu_3O_{7-x}$ phase are close to those for more fully oxidized $YBa_2Cu_3O_{7-x}$. Recent theoretical results also suggest that higher resistivity materials such as nonsuperconducting Y-Ba-Cu-O may be more suitable for obtaining high I_cR_n products than metals such as Au or Ag.[15,16]

We utilize an edge geometry[8,11,12,17] for this work, because this device structure has a number of important advantages over other possible geometries such as sandwich and lateral geometry devices. The basic device structure is formed by depositing the N-YBaCuO layer and the $YBa_2Cu_3O_{7-x}$ counterelectrode on the exposed edge of a c-axis-oriented $YBa_2Cu_3O_{7-x}$ thin film overlayed by a thick insulator. This geometry allows small device areas and very short microbridge lengths to be achieved using conventional photolithography. The edge geometry also has the advantages that, for c-axis $YBa_2Cu_3O_{7-x}$ films, the current flow in the device active area and lead-in electrodes is along the high current density a-b planes, and that the critical normal-superconductor device interfaces are located on the longer coherence length surfaces perpendicular to the a-b planes.

The growth conditions for the superconducting and nonsuperconducting Y-Ba-Cu-O thin films used in these experiments were nominally identical except for the substrate temperature and the deposition rate. The Y-Ba-Cu-O films were deposited by pulsed excimer laser ablation at 248 nm and an energy density of 1 J/cm^2. The oxygen pressure during deposition was 200 mT, and the deposition rate was $\approx$1.7 Å/pulse. The thin N-YBaCuO layers were grown at a laser repetition rate of 1 Hz, while the thicker superconducting layers were grown at 5 Hz. The backing plate temperature during growth of the nonsuperconducting Y-Ba-Cu-O films was approximately 520–540 °C, and about 790–810 °C during growth of the base and counterelectrode layers. For device runs, the Y-Ba-Cu-O barrier deposition was immediately followed by a ramp to the higher growth temperature, the counterelectrode was deposited, and the layers were then annealed in 50 T of oxygen at $\approx$500 °C for 12 min. This annealing procedure was also used for the base electrode films. Typical film thicknesses are 25–100 Å for the N-YBaCuO, and 1500–3000 Å for the superconducting electrodes.

The nonsuperconducting Y-Ba-Cu-O films have not been extensively characterized to date, in part due to the difficulty of obtaining quantitative information on very thin films grown on small area $YBa_2Cu_3O_{7-x}$ edges. However, lateral transport resistance versus temperature measurements have been made on 100-Å-thick Y-Ba-Cu-O films grown on $LaAlO_3$ substrates at 520–540 °C, which were then heated to $\approx$800 °C for one minute to simulate the counterelectrode growth conditions. In this case it is found that the Y-Ba-Cu-O resistivity initially increases and then decreases as the temperature is reduced, with values of

 0003-6951/91/330982-03$02.00

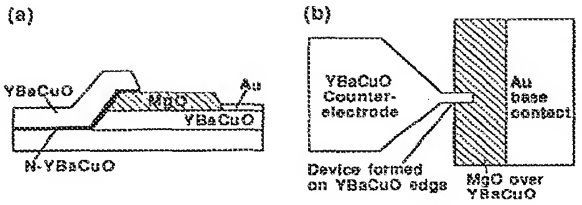

FIG. 1. Schematic diagrams of an edge-geometry $YBa_2Cu_3O_{7-x}$/N—YBaCuO/$YBa_2Cu_3O_{7-x}$ device structure. (a) Side view, (b) top view.

$\simeq$7–15 mΩ cm near 4.2 K. However, some films prepared under nominally similar conditions exhibit semiconductor-like behavior with resistivities of 200–300 mΩ cm below 10 K. Although the laser ablation process presumably reproduces the 1:2:3 Y:Ba:Cu stoichiometry of our target, at this point the oxygen stoichiometry and structure of these Y-Ba-Cu-O layers is not known.

The edge-geometry device processing steps are briefly outlined here with schematic side and top views of a completed device shown in Fig. 1. The fabrication process begins with the deposition of the $YBa_2Cu_3O_{7-x}$ base electrode film on a $LaAlO_3$ substrate. A thick MgO film is then patterned by photolithography and liftoff. The MgO layer is utilized as an ion milling mask to define a self-aligned edge in the base electrode using 500 eV Ar ions, followed by a brief 50 eV Ar ion edge cleaning. Immediately after this step, within the same vacuum system, the substrate temperature is increased and the N-YBaCuO barrier layer and $YBa_2Cu_3O_{7-x}$ counterelectrode are deposited. After annealing, a second lithography and ion milling step is used to cut via holes through the MgO to the base electrode and liftoff Au pads. Finally, a third lithography and ion milling process defines the counterelectrode patterns. There are nine devices per chip with nominal counterelectrode tip widths of 10 and 15 μm. To date this process has had a perfect yield, with all 54 devices on the first 6 chips exhibiting well-defined supercurrents.

The best results were obtained with edge-geometry weak links having 50-Å-thick Y-Ba-Cu-O barrier layers at temperatures above 50 K. A typical I-V characteristic at 61.5 K for such a device is shown in Fig. 2(a). The I-V curve is qualitatively consistent with the RSJ model, unlike the piecewise-linear or flux-flow characteristics often observed with other all high T_c weak links. This particular weak link had a current density of 6.5 kA/cm^2 and an I_cR_n product of 105 μV at this temperature, while at 4.2 K the I_cR_n product increased to 0.66 mV. Although these I_cR_n products are smaller than predicted,[15] larger I_cR_n values may result from improvements in counterelectrode overgrowth. Another point to note is that the resistance of this 11 μm$\times$0.28 μm device is $\simeq$0.5 Ω, so that 5 Ω device resistances should be achievable with 1 μm lithography, and 50 Ω with 0.1 μm lithography. As shown in Fig. 2(b), these devices exhibited strong microwave response, with ac Josephson steps at the expected voltages ($V_n = nh\nu/2e$) under 10 GHz microwave irradiation. The microwave step

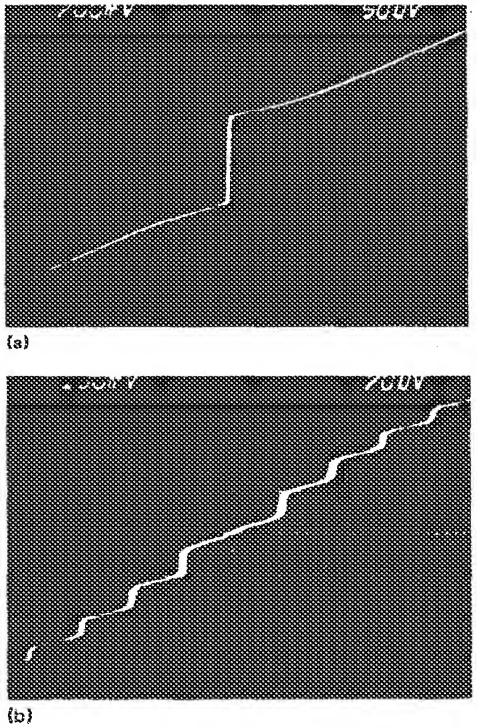

FIG. 2. I-V characteristics at 61.5 K for an all high T_c edge-geometry weak link with a 50 Å N-YBaCuO barrier layer. (a) No applied microwave radiation. (Vertical) 200 μA/div, (Horizontal) 50 μV/div. (b) ac Josephson steps under 10.0 GHz microwave irradiation. The rf power is such that critical current has been completely suppressed. (Vertical) 100 μA/div, (Horizontal) 20 μV/div.

amplitudes showed Bessel-function-like oscillatory behavior with increasing rf field, qualitatively consistent with a RSJ current source model.[18] At 4.2 K the 50 Å barrier devices had current densities of about 10^5 A/cm^2, but showed less ideal device characteristics, with flux-flow-type I-V curves and weak microwave response. The nonideal I-V characteristics in this case may be due to self-shielding effects related to the small Josephson penetration depth (λ_J) in these high J_c, relatively wide junctions.

Devices with 25- and 100-Å-thick Y-Ba-Cu-O barrier layers were also tested. At 4.2 K and higher temperatures the weak links with 100 Å barriers sometimes exhibited RSJ-like I-V characteristics, but many of the devices had nonideal piecewise-linear I-V curves. Some of these devices showed ac Josephson steps which modulated completely with increasing rf power, but typically the magnetic field modulation of the critical currents was less than 30%. The 25 Å barrier devices often showed RSJ I-V characteristics at higher temperatures with strong microwave response up to $\sim$85 K. However, these weak links also showed incomplete ($<$70%) magnetic field modulation and exhibited hysteresis and switching noise at low voltages, which may be related to switching of weak spots or pinholes in these very thin barriers. In contrast to the 25 and 100 Å barrier devices, above 50 K the 50 Å barrier weak links typically

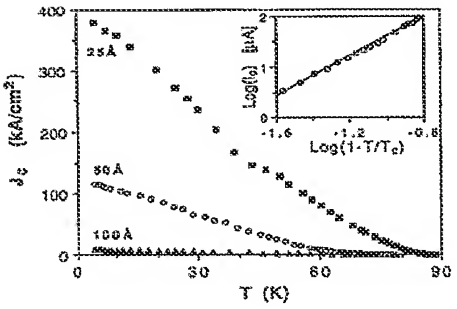

FIG. 3. Critical current density vs temperature for all high T_c weak links with N-YBaCuO barrier thicknesses of 25, 50, and 100 Å. The inset is a plot of $\log(I_c)$ vs $\log(1 - T/T_c)$ for the 50 Å barrier device near T_c with a curve fit giving a slope of 2.0.

showed 80%–100% critical current modulation in applied magnetic fields. The I_c vs B data for such devices exhibited diffraction patterns approximating the expected Fraunhofer behavior, with a strong central peak and periodic I_c modulation, but with some asymmetry in the pattern, indicating fairly good barrier uniformity. In these preliminary magnetic field measurements, the field was not applied parallel to the junction base electrode edge, so quantitative determination of the effective device area is not possible.

Another important indicator of the uniformity of the Y-Ba-Cu-O barrier layers is the scaling behavior of the critical current and device resistance with barrier thickness and device area. The temperature dependence of the critical current density for devices with 25, 50, and 100 Å barrier thicknesses is shown in Fig. 3. The qualitative shape of the J_c vs T curves is similar for all three barrier thicknesses, and a fit of the data for the 50 Å barrier device (see inset of Fig. 3) indicates that I_c goes as $(1 - T/T_c)^2$ near T_c as predicted by basic theories for superconductor/normal-metal/superconductor (SNS) devices.[19] Figure 3 clearly shows the strong dependence of critical current on barrier thickness with J_c at 4.2 K ranging from 8.3×10^3 A/cm^2 for the 100 Å barrier, to 3.8×10^5 A/cm^2 for the 25 Å barrier. A plot of $\ln J_c$ vs barrier thickness L at 4.2 K (not shown) indicates that, to a very good approximation, J_c goes as $\exp(-L/\xi_n)$, where $\xi_n = 20$ Å is the effective normal metal coherence length for the N-YBaCuO layer. Such exponential scaling of J_c with the normal metal barrier thickness is also predicted by simple theories of SNS behavior.[19] These devices also show resistances which scale inversely with the device area, and average R_nA products which scale approximately linearly with the barrier thickness: the average R_nA products at 4.2 K for the 25, 50, and 100 Å barrier thicknesses are 2.7×10^{-9}, 7.7×10^{-9}, and 1.2×10^{-8} Ω cm^2, respectively. The scaling of J_c and R_n with barrier thickness and device area indicates that the Y-Ba-Cu-O barrier layers are indeed relatively uniform, and that the device behavior is not dominated by pinhole conduction. In contrast to the lateral resistivity measurements of N-YBaCuO films on $LaAlO_3$ substrates, preliminary tests show a factor of 2–3 decrease in device resistance as the temperature is lowered from $\approx$80 to 4.2 K. However, the magnitudes of the device R_nA products are consistent with the low end of the resistivity range seen in the lateral transport experiments.

In summary, high quality, all high T_c edge-geometry weak links have been fabricated using nonsuperconducting Y-Ba-Cu-O barrier layers and a device process with excellent yield. The best results are obtained with devices incorporating 50 Å barrier layers, which show RSJ-like I-V characteristics with strong ac and dc Josephson effects. The scaling behavior of J_c and R_n with barrier thickness and area indicates that the Y-Ba-Cu-O barrier layers form uniform, high quality weak links with an effective normal metal coherence length of 20 Å at 4.2 K.

The research described in this letter was performed by the Center for Space Microelectronics Technology, Jet Propulsion Laboratory, California Institute of Technology, and was jointly sponsored by the National Aeronautics and Space Administration, Office of Aeronautics, Exploration, and Technology, by the Defense Advanced Research Projects Agency, and by the Strategic Defense Initiative Organization, Innovative Science and Technology Office.

[1]J. Mannhart, P. Chaudhari, D. Dimos, C. C. Tsuei, and T. R. McGuire, Phys. Rev. Lett. 61, 2476 (1988).
[2]S. E. Russek, D. K. Lathrop, B. H. Moeckly, R. A. Buhrman, D. H. Shin, and J. Silcox, Appl. Phys. Lett. 57, 1155 (1990).
[3]R. W. Simon, J. B. Bulman, J. F. Burch, S. B. Coons, K. P. Daly, W. D. Dozier, R. Hu, A. E. Lee, J. A. Luine, C. E. Platt, S. M. Schwarzbek, M. S. Wire, and M. J. Zani, IEEE Trans. Magn. 27, 3209 (1991).
[4]D. B. Schwartz, P. M. Mankiewich, R. E. Howard, L. D. Jackel, B. L. Straughn, E. G. Burkhart, and A. H. Dayem, IEEE Trans. Magn. 25, 1298 (1989).
[5]M. G. Forrester, J. Talvacchio, J. R. Gavaler, M. Rooks, and J. Lindquist, IEEE Trans. Magn. 27, 3098 (1991).
[6]M. S. Wire, R. W. Simon, J. A. Luine, K. P. Daly, S. B. Coons, A. E. Lee, R. Hu, J. F. Burch, and C. E. Platt, IEEE Trans. Magn. 27, 3106 (1991).
[7]C. T. Rogers, A. Inam, M. S. Hegde, B. Dutta, X. D. Wu, and T. Venkatesan, Appl. Phys. Lett. 55, 2032 (1989).
[8]J. Gao, W. A. Aarnink, G. J. Gerritsma, D. Veldhuis, and H. Rogalla, IEEE Trans. Magn. 27, 3062 (1991).
[9]D. K. Chin and T. Van Duzer, Appl. Phys. Lett. 58, 753 (1991).
[10]K. Mizuno, K. Higashino, K. Setsune, and K. Wasa, Appl. Phys. Lett. 56, 1469 (1990).
[11]R. B. Laibowitz, R. H. Koch, A. Gupta, G. Koren, W. J. Gallagher, V. Foglietti, B. Oh, and J. M. Viggiano, Appl. Phys. Lett. 56, 686 (1990).
[12]G. Koren, E. Aharoni, E. Polturak, and D. Cohen, Appl. Phys. Lett. 58, 634 (1991).
[13]J. D. Jorgensen, B. W. Veal, A. P. Paulikas, L. J. Nowicki, G. W. Crabtree, H. Claus, and W. K. Kwok, Phys. Rev. B 41, 1863 (1990).
[14]I. A. Agostinelli, S. Chen, and G. Braunstein, Phys. Rev. B 43, 11396 (1991).
[15]G. Deutscher and R. W. Simon, J. Appl. Phys. 69, 4137 (1991).
[16]M. Y. Kupriyanov and K. K. Likharev, IEEE Trans. Magn. 27, 2460 (1991).
[17]B. D. Hunt, M. C. Foote, and L. J. Bajuk, IEEE Trans. Magn. 27, 848 (1991).
[18]T. Van Duzer and C. W. Turner, *Principles of Superconductive Devices and Circuits* (Elsevier/North Holland, New York, 1981), pp. 180–185.
[19]P. G. DeGennes, Rev. Mod. Phys. 36, 225 (1964).

USSN 10/751,091

EVIDENCE APPENDIX

ATTACHMENT B.2

US005945383A

United States Patent [19]

Hunt

[11] Patent Number: 5,945,383

[45] Date of Patent: Aug. 31, 1999

[54] **METHOD PRODUCING AN SNS SUPERCONDUCTING JUNCTION WITH WEAK LINK BARRIER**

[75] Inventor: **Brian D. Hunt**, Pasadena, Calif.

[73] Assignee: **The United States of America as represented by the Administrator of the National Aeronautics and Space Administration**, Washington, D.C.

[21] Appl. No.: **07/854,124**

[22] Filed: **Mar. 19, 1992**

[51] **Int. Cl.**[6] **H01L 39/24**

[52] **U.S. Cl.** **505/329**; 505/474; 505/190; 505/702; 505/732; 427/62

[58] **Field of Search** 505/1, 702, 701, 505/732, 329, 190, 474; 427/62, 63, 53.1, 419.3, 596; 257/33, 34

[56] **References Cited**

U.S. PATENT DOCUMENTS

4,891,355	1/1990	Hayashi et al.	505/1
5,034,374	7/1991	Awaji et al.	505/1
5,047,390	9/1991	Higashino et al.	505/1
5,221,661	6/1993	Housley .	

FOREIGN PATENT DOCUMENTS

63252316 10/1988 Japan .

OTHER PUBLICATIONS

Dijkkamp et al, Appl. Phys. lett. 51(8), Aug. 1987, pp. 519–520.

B.D. Hunt et al. (Hunt), "All high T_c edge–geometry weak links utilizing Y–Ba–Cu–0 barrier layers," *Appl. Phys. Lett.*, No. 8, pp. 982–984 (Aug. 1991).

J.A. Agostinelli et al. (Agostinelli), "Cubic phase in the Y–Ba–Cu–0 system," 43 *Phys. Rev. B*, No. 13, 11, pp. 396–399 (May 1, 1991).

Wu et al, "Effect of deposition rate on properties of $Y_1Ba_2Cu_3O_{7-\delta}$ superconducting thin films," Appl. Phys. lett. 56(15) Apr. 1990 pp. 1481–1483.

Gao et al, "Controlled preparation of all high–T_c SNS–type edge junctions and DC SQUIDs", Physica C 171 (1990) pp. 126–130 No month data!

Rogers et al, "Fabrication of heteroepitaxial $YBa_2Cu_3O_{7-x}$–$PrBa_2Cu_3O_{7-x}$–$YBa_2Cu_3O_{7-x}$ Josephson devices grown by laser deposition", Appl. Phys. lett. 55 (19) Nov. 1989 pp. 2032–2034.

Krebs et al, "Conditions for oriented growth of Y–Ba–Cu–O and Bi–Sr–Ca–Cu–O films by pulsed laser ablation", J. Appl. Phys. 69(4) Feb. 1991 pp. 2405–2409.

Yoshida et al, "Monolithic device fabrication using high–Tc superconductor", International Electron Devices Meeting (IEDM) (Sanfrancisco, CA) Dec. 11–14, 1988 pp. 282–285.

Koren et al, "Highly oriented as–deposited superconducting laser ablated thin films of $Y_1Ba_2Cu_3O_{7-\delta}$ on $SrTiO_3$, Zirconia, and Si substrates" Appl. Phys. lett. 53(23) Dec. 1988 pp. 2330–2332.

"High Temperature Superconductor Josephson Weak Links," by Brian D. Hunt et al, Electrochemical Society Meeting, Honolulu, Hawaii, May 17–21, 1993 No page data!

"Cubic Phase in the Y–Ba–Cu–O Stystem", Agostinelli et al., Physics Review B 43, p. 11396, (1991) No month data!

Primary Examiner—Roy V. King
Attorney, Agent, or Firm—John H. Kusmiss

[57] **ABSTRACT**

A method of producing a high temperature superconductor Josephson element and an improved SNS weak link barrier element is provided. A YBaCuO superconducting electrode film is deposited on a substrate at a temperature of approximately 800° C. A weak link barrier layer of a nonsuperconducting film of N—YBaCuO is deposited over the electrode at a temperature range of 520° C. to 540° C. at a lower deposition rate. Subsequently, a superconducting counter-electrode film layer of YBaCuO is deposited over the weak link barrier layer at approximately 800° C. The weak link barrier layer has a thickness of approximately 50 Å and the SNS element can be constructed to provide an edge geometry junction.

27 Claims, 6 Drawing Sheets

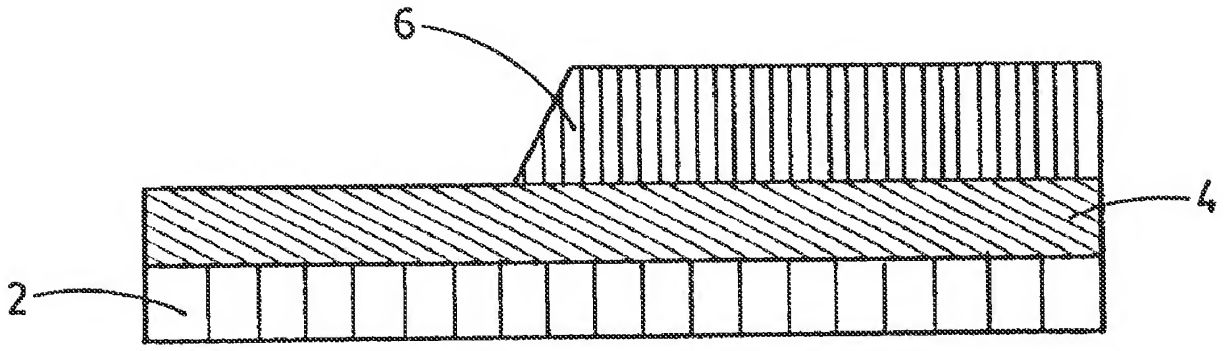

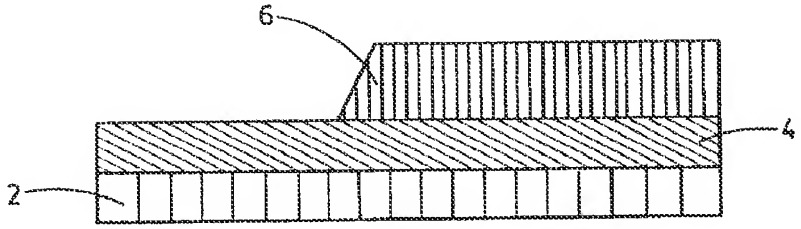

FIG. 1

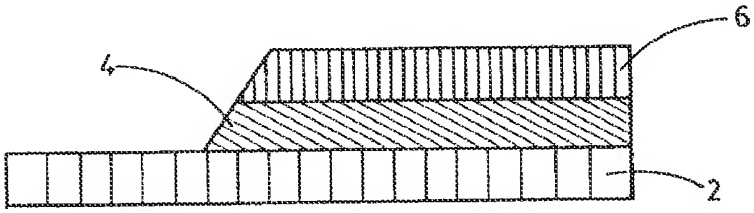

FIG. 2

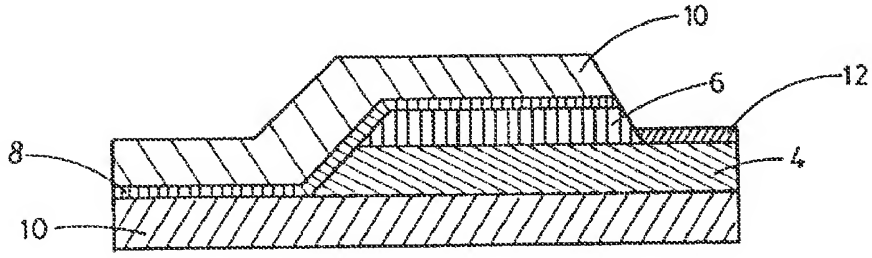

FIG. 3

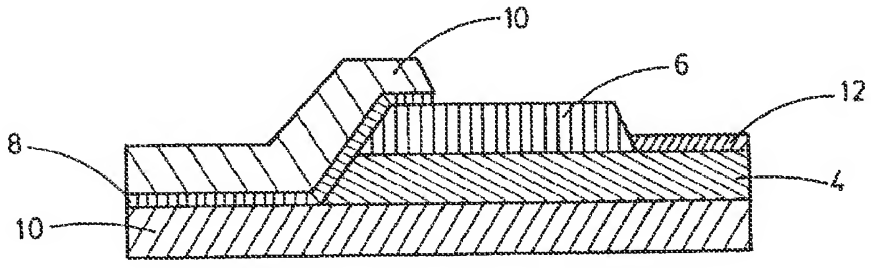

FIG. 4

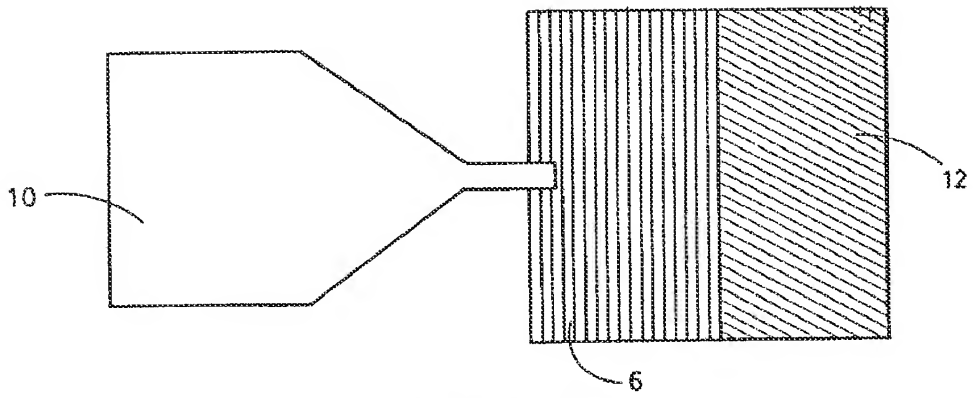

FIG. 5

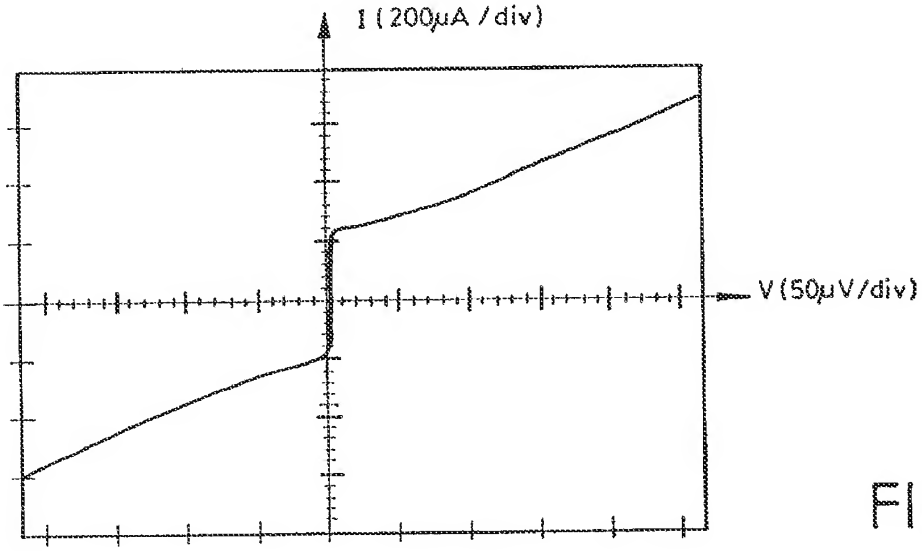

FIG. 6

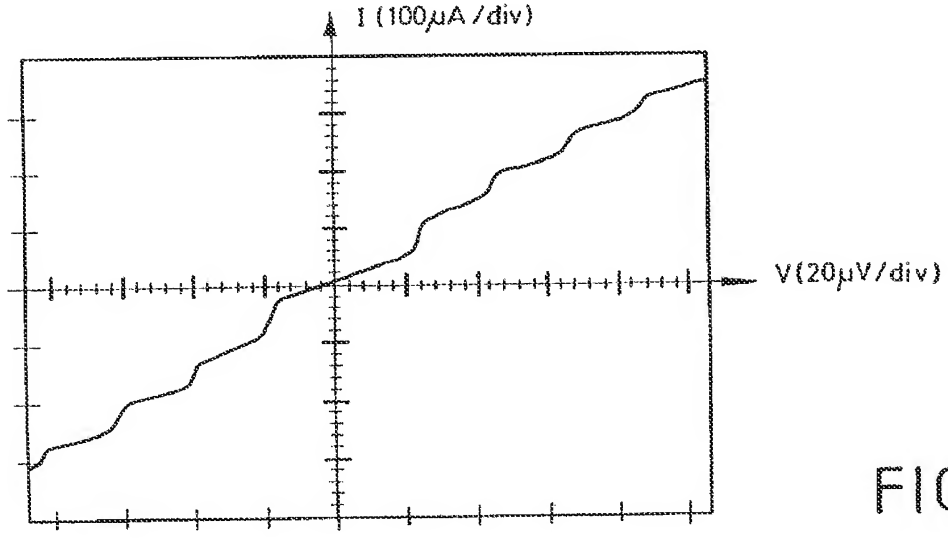

FIG. 7

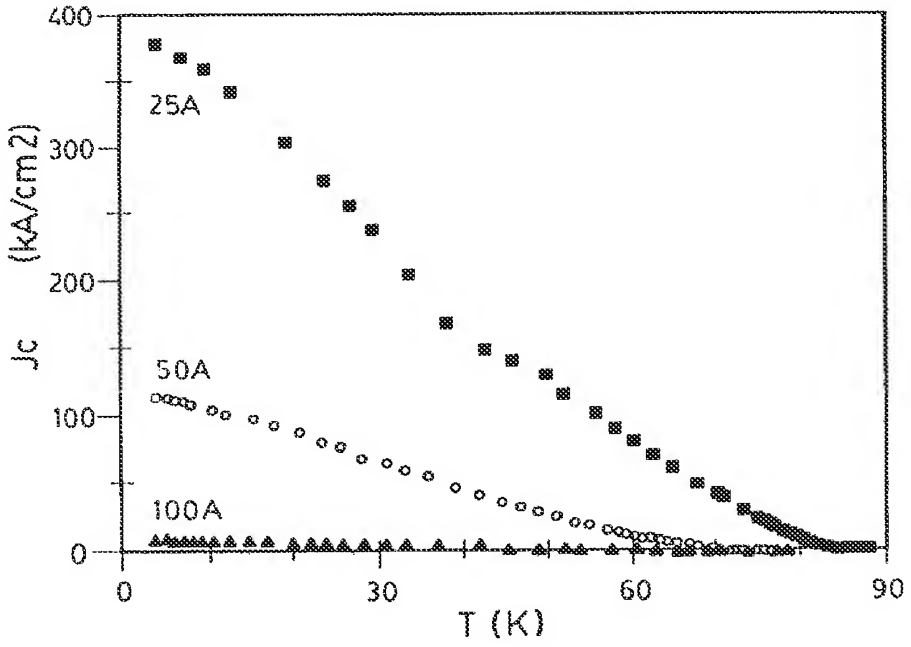
400
300
200
100
0
Jc (kA/cm2)
25A
50A
100A
0
30
60
90
T (K)

FIG. 8

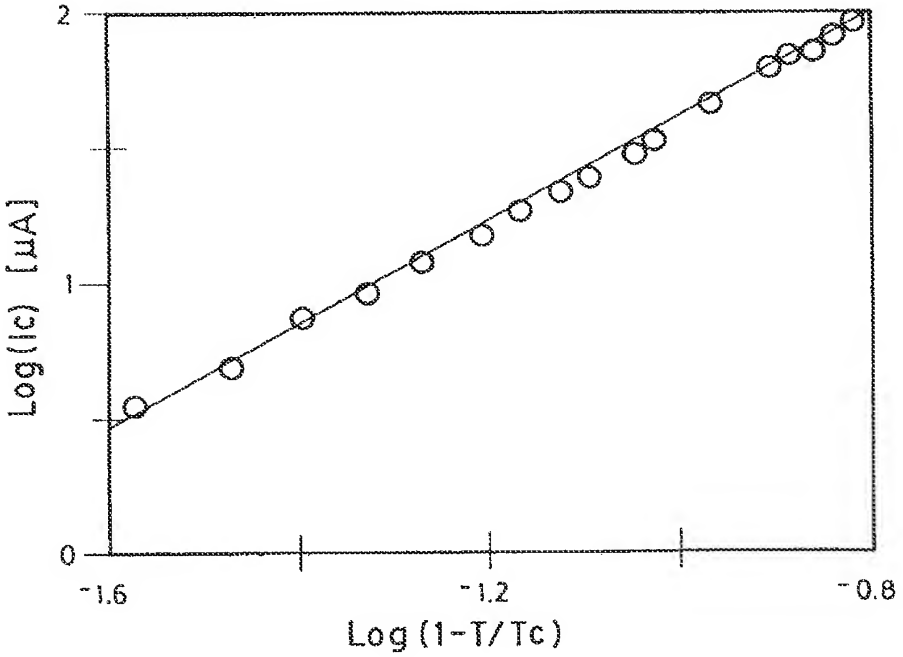
2
1
0
Log (Ic) [μA]
-1.6
-1.2
-0.8
Log (1-T/Tc)

FIG. 9

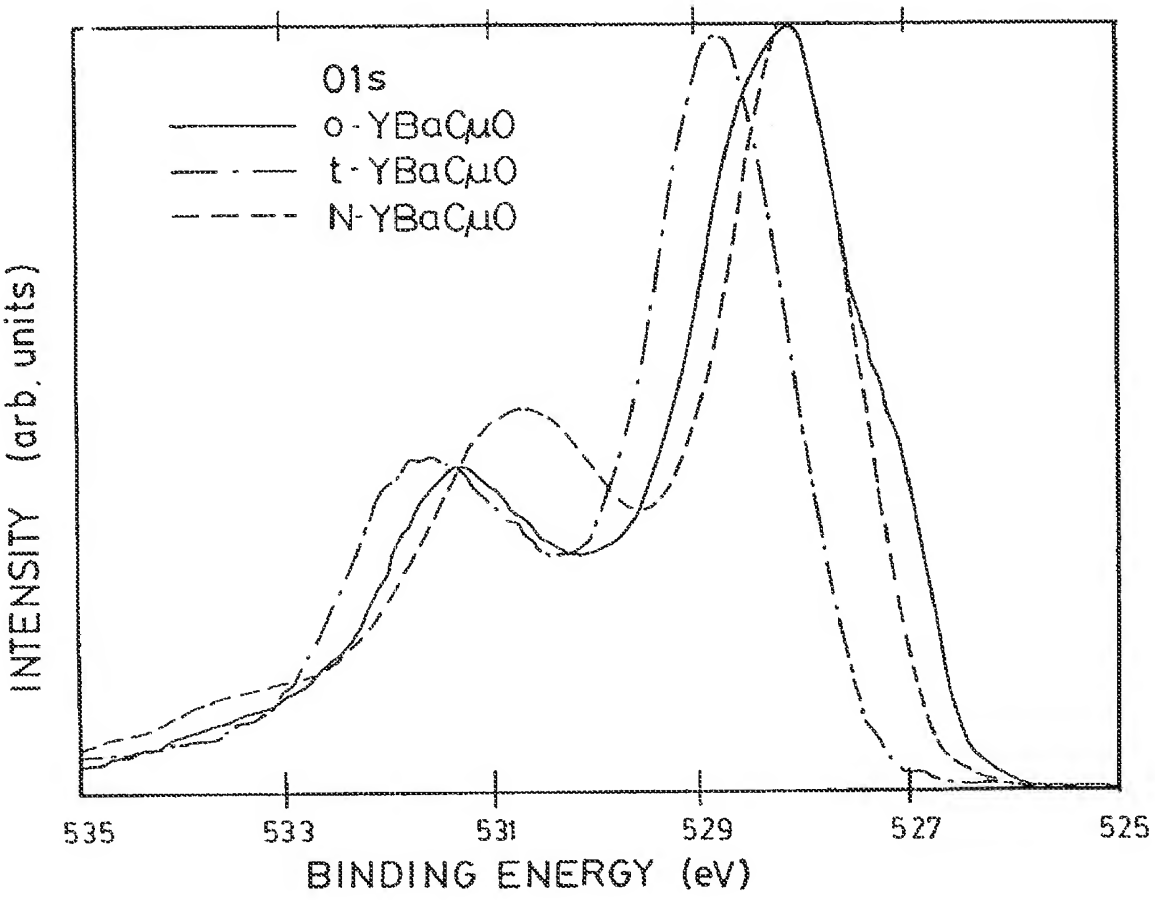
01s
o-YBaCuO
t-YBaCuO
N-YBaCuO
INTENSITY (arb. units)
535
533
531
529
527
525
BINDING ENERGY (eV)

FIG. 10

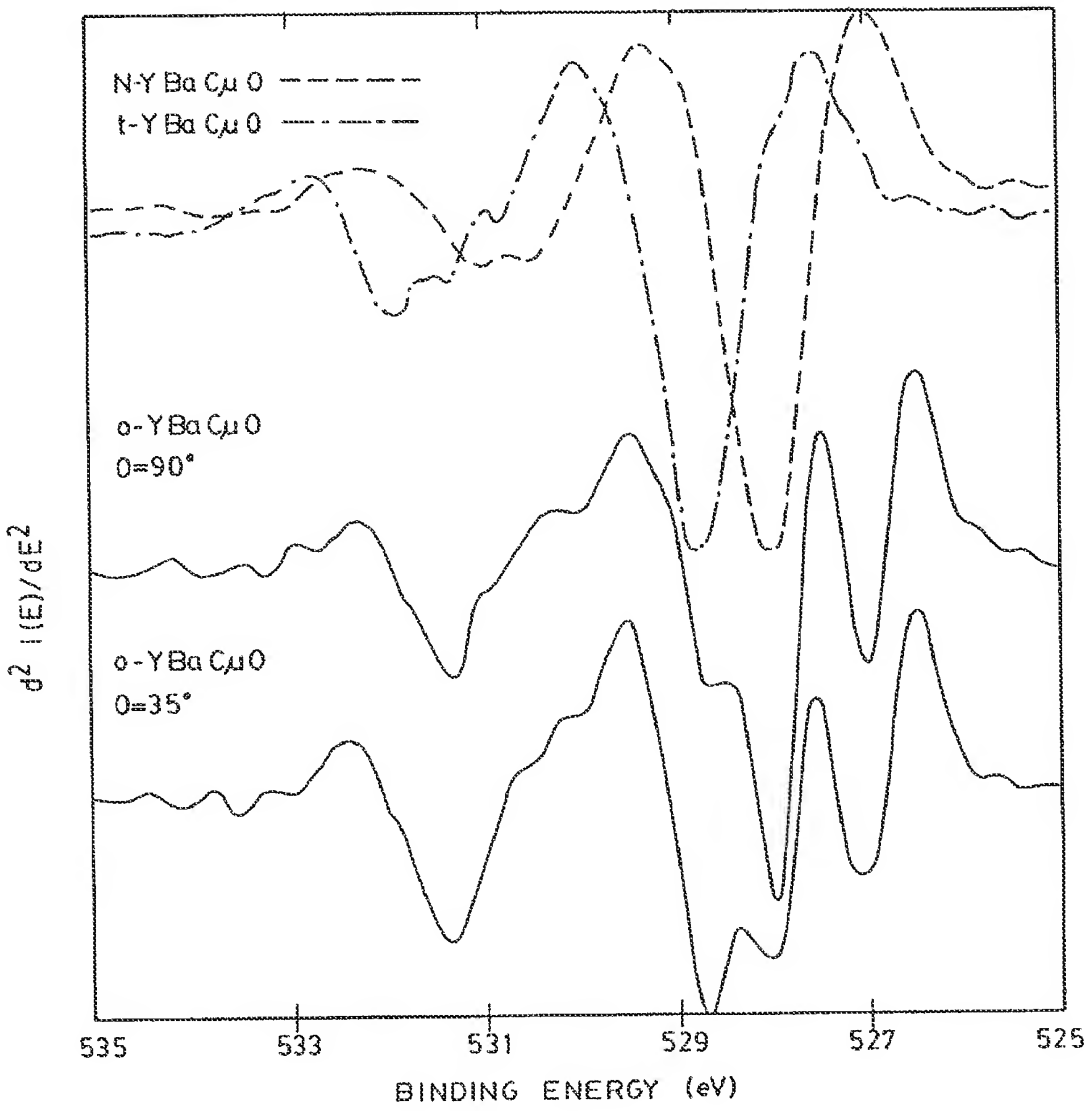
N-Y Ba Cμ 0
t-Y Ba Cμ 0
o-Y Ba Cμ 0
θ=90°
o-Y Ba Cμ 0
θ=35°
d² I(E)/dE²
535
533
531
529
527
525
BINDING ENERGY (eV)

FIG. 11

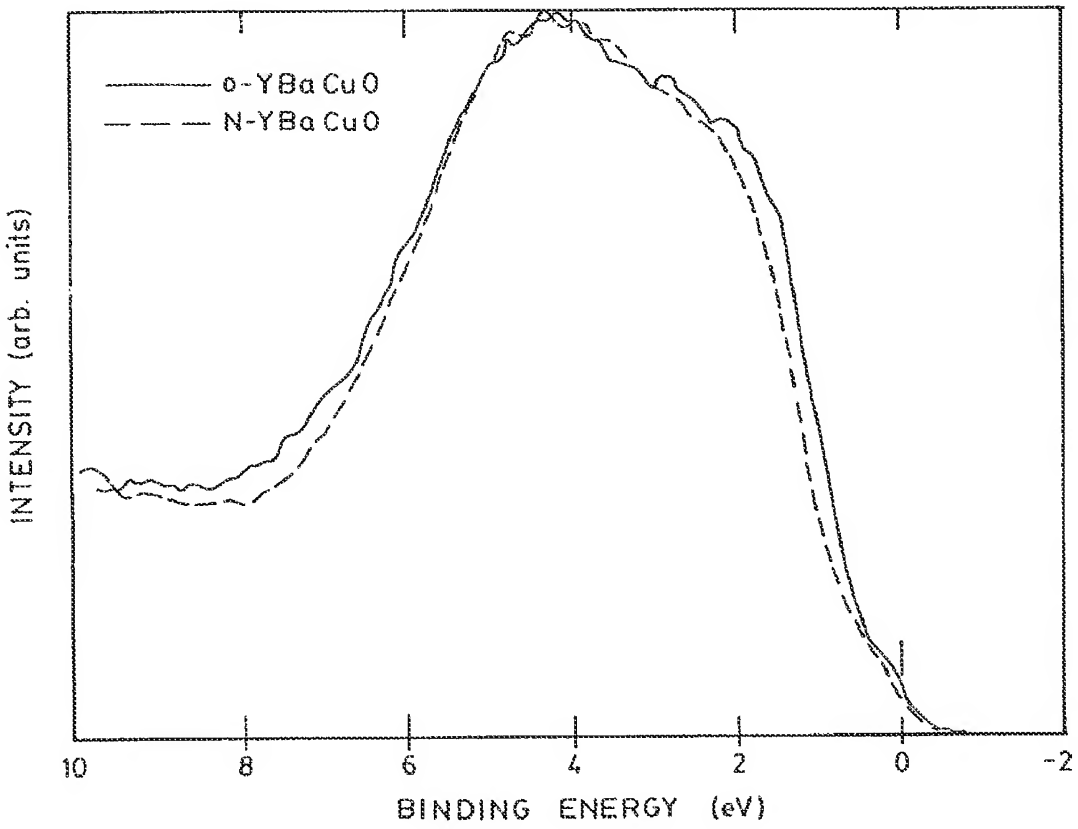
o-YBa Cu O
N-YBa Cu O
INTENSITY (arb. units)
10
8
6
4
2
0
-2
BINDING ENERGY (eV)

FIG. 12

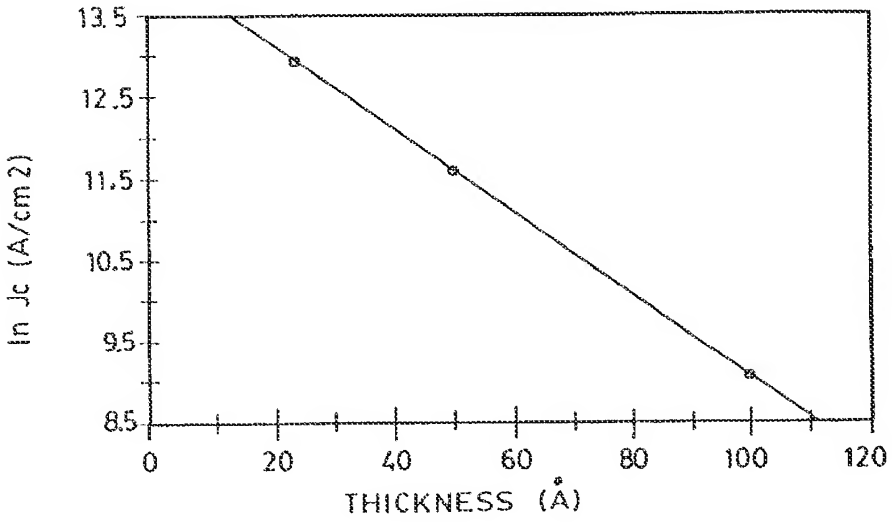
13.5
12.5
11.5
10.5
9.5
8.5
ln Jc (A/cm 2)
0
20
40
60
80
100
120
THICKNESS (Å)

FIG. 13

METHOD PRODUCING AN SNS SUPERCONDUCTING JUNCTION WITH WEAK LINK BARRIER

ORIGIN OF THE INVENTION

The invention described herein was made in the performance of work under a NASA contract, and is subject to the provisions of Public Law 96-517 (35 U.S.C. Section 202) in which the Contractor has elected not to retain title.

TECHNICAL FIELD

The present invention is directed to a high temperature superconductor junction produced from a family of rare earth-alkaline earth-cuprate superconductors, and more particularly to an SNS structure having a weak link barrier of a structure compatible with growth on a first superconductor electrode and consistent with providing a good, uniform layer interface for growth of a second superconductor electrode and a method of producing the same.

BACKGROUND ART

The investigation of superconductor devices has been extremely active in recent years because of the potential benefits that can be achieved if their performance and production methods can be made practical for reliable and economical applications in the electronic fields. A tunnel junction and microbridge are the two basic active Superconductor devices which exhibit the ac and dc Josephson effects are required for many applications. Although tunnel junctions fabricated from the conventional, low temperature superconductors have proven to be quite useful, severe surface and interface problems have prevented the successful fabrication of high quality, high temperature superconductor tunnel junctions to date. The extremely short coherence lengths in $YBa_2Cu_3O_{7-x}$, ~2--15 Å, place stringent requirements on the quality of the tunnel barrier material and its interfaces in superconductor-insulator-superconductor (SIS) device structures. These requirements include that the barrier material be extremely thin (~10--20 Å), pin hole free, chemically compatible with the superconductor, and that the superconducting energy gap be fully developed within a coherence length of the interfaces.

The fabrication of high Tc superconductor/normal metal/superconductor (SNS) microbridges are believed to be less difficult to fabricate than tunnel junctions, due to fewer problems with material interaction and because the normal metal weak link layers can be thicker and hence more easily controllable than the typical tunnel barriers. The stringent requirements for SIS structures are thus somewhat relaxed for SNS structures, though the requirement of high quality interfaces remains. Unfortunately, high quality interfaces are difficult to attain since most metals are reactive with orthorhombic YBaCuO, (o-YBaCuO) and use of a nonreactive Ag or Au makes growth of a high quality of o-YBaCuO counterelectrode difficult due to the mismatch between the o-YBaCuO and Ag or Au crystal lattices.

All high Tc Josephson weak links are potentially useful for high frequency sources and detectors, for high speed, low power digital logic, and for sensitive magnetic field detectors. For optimal performance in these applications, certain device characteristics are desirable, including large (<1 mV) values of the critical current-normal state resistance product (I_cR_n) accompanied by strong ac and dc Josephson response, device resistances on the order of 50 Ω, and high critical current densities (J_c) for high speed operation. A great deal of effort has been focused on obtaining useful all high Tc Josephson devices with published reports on a wide variety of device structures. The various junction geometries that have been studied include grain boundary weak links as reported in Mannhart et al. "Critical Currents in [001] Grains and Across Their Tilt Boundaries, in $YBa_2Cu_3O_7$ Film", Phys. Rev. Lett. 61, pg. 2476 (1988) and Russek et al. "Scaling Behaviour of $YBa_2Cu_3O_{7-x}$ Thin Film Weak Links", Appl. Phys. Lett. 57, pg. 1155 (1990), all $YBa_2Cu_3O_{7-x}$ step edge microbridges, see Simon et al., "Engineered HTS Microbridges", IEEE Trans. Magnetics 27, pg. 3209 (1991), Au or Ag-coupled microbridges, and epitaxial sandwich or edge-geometry structures using barriers such as $PrYBa_2Cu_3O_{7-x}$, Bn-doped $SrTiO_3$, $Bi_2Sr_2CuO_y$, or CF_4 treated $YBa_2Cu_3O_{7-x}$, see Gao et al, "Preparation and Properties of All High T_c SNS-Type Edge DC Squids", IEEE Trans Magnetics 27, pg 3062 (1991), Chin et al., "Novel All-High T_c Epitaxial Josephson Junction", Appl. Phys. Lett. 58, pg. 753 (1991), Mizuno et al., "Fabrication of Thin-Film-Type Josephson Junctions Using a Bi—Cr—Ca—Cu—O/Bi—Sr—Cu—O/Bi—Sr—Ca—Cu—O Structure", Appl. Phys. Lett. 56, pg 1469 (1990), and Koren et al., "Properties of all $YBa_2Cu_3O_{7-x}$ Josephson Edge Junctions Prepared by in situ Laser Ablation Deposition", Appl. Phys. Lett. 58, pg. 634 (1991). Although progress has been made with these devices, their electrical characteristics are often less than ideal with many devices suffering from one or more of the following problems: 1) current-voltage (I-V) characteristics inconsistent with the resistively-shunted junction (RSJ) model; 2) weak magnetic field and microwave response; and 3) low I_cR_n products (<500 μV).

U.S. Pat. No. 4,891,355 discloses a method of producing a superconducting circuit, wherein a laser beam is used to form nonsuperconducting barrier regions between superconducting portions of the film. These barrier regions appear to electrically separate various superconducting parts of the circuit and the dimension of the nonsuperconducting segments will be limited to the dimensions of the laser wavelengths, due to diffraction effects. In essence, a film of a ceramic superconductive material is deposited on a substrate in a superconducting state and then exposed to the laser beam as part of a high temperature heat treatment to turn it into a nonsuperconducting state.

An article "Cubic Phase in the Y—Ba—Cu—O System" by Agostinelli et al., Physics Review B 43, pg. 11396 (1991), discloses a cubic phase of a rare earth-alkaline earth-cuprate film that was deposited as a thin film on a single crystal magnesium oxide substrate by excimer laser ablation.

U.S. Pat. No. 5,034,374 teaches a method of producing a high temperature superconductor element formed from rare earth-alkaline earth-cuprate superconductors with an insulating layer formed between the lower and upper ceramic high temperature superconductor films by an interdiffusion of ceramic superconductors to thereby form a tunnel junction exhibiting Josephson effects.

U.S. Pat. No. 5,047,390 discloses another configuration of a tunnel junction Josephson device.

Finally, the Japanese laid-open patent application No. 63-252316 apparently refers to the deposition of a barrier layer between a substrate and a superconducting material.

The prior art is still seeking to provide an optimum superconducting device exhibiting Josephson effects that can be efficiently manufactured with high yield.

STATEMENT OF THE INVENTION

The present invention discloses a method of providing a high temperature superconductor Josephson element and a

novel Josephson element having a weak link barrier layer of a non-superconducting film in a family of rare earth-alkaline earth-cuprate superconductors. An appropriate substrate, such as $LaAlO_3$, is prepared and a film layer of $YBa_2Cu_3O_{7-x}$ is deposited as a base electrode on the substrate by a pulsed excimer laser ablation technique in a vacuum chamber with an oxygen environment of approximately 100–200 m Torrs. The backing plate temperature was approximately 790°–830° C. during the growth of the base electrode superconducting layer. The base electrode layer is annealed in 50–100 Torrs of oxygen for approximately 12 minutes at about 500° C. Subsequently, a thick insulating layer, such as magnesium oxide was deposited and patterned by a photolithography and lift-off process. The magnesium oxide layer was utilized as an ion milling mask to define a self-aligning edge in the base superconductor electrode. An ion milling and cleaning step created an edge in the base superconductor electrode. A weak link barrier layer of a nonsuperconducting film of Y----Ba----Cu----O ("N----YBaCuO") is then deposited across the base electrode edge at a reduced temperature of approximately 520–540° C. Again, a laser ablation vacuum deposition procedure at 100–200 m Torrs was utilized and the deposition rate was substantially reduced by limiting the laser repetition rate to 1 Hz compared to the 5 Hz that was utilized for the base electrode superconductor layer. Subsequently, the temperature of the backing plate was increased to approximately 800° C. and a superconducting counter-electrode layer of $Yba_2Cu_3O_{7-x}$ was deposited at a laser repetition rate of 5 Hz. The resulting structure was then annealed in 50–100 Torrs of oxygen at approximately 500° C. for 12 minutes. The junction was then subject to a second lithography and ion milling step to cut holes through the magnesium oxide to the base electrode and lift-off gold pads. A third lithography and ion milling process define the specific counter-electrode patterns that were desired.

This method produced a high Tc edge geometry weak link superconductor Josephson element of an SNS device structure having a weak link barrier layer within a range of approximately 5 Å to 200 Å in thickness with a base electrode and counter-electrode of approximately 1000 Å to 3500 Å in film thickness. Preferably, the weak link layer thickness is in the range of 25 Å to 100 Å with a preferred embodiment having a thickness of approximately 50 Å and an effective metal coherence length of 20 Å at a temperature of 4.2 K.

Tests have indicated that the weak link layer provided a very good SNS device with a current-voltage curve characteristic consistent with the desired RSJ model and 80–100% critical current modulation in applied magnetic fields. As can be appreciated, the weak link barrier layer may have a relative close lattice match to the superconducting YBaCuO electrodes, with a similar crystal structure, and is obviously chemically compatible with the superconductor electrodes at their growth temperature. The weak link normal metal layer grew in a two-dimensional fashion with relatively few pin holes and had a relative long coherence length with a high restivity that would suggest the capacity for appropriate scaling to 50 Ω with 0.1 μm lithography.

BRIEF DESCRIPTION OF THE DRAWINGS

The objects and features of the present invention, which are believed to be novel, are set forth with particularity in the appended claims. The present invention, both as to its organization and manner of operation, together with further objects and advantages, may best be understood by reference to the following description, taken in connection with the accompanying drawings.

FIG. **1** is a schematic cross-sectional configuration of the structure in one step in producing the edge geometry configuration;

FIG. **2** is a schematic cross-sectional configuration illustrating an interim configuration of the structure;

FIG. **3** is a schematic cross-sectional configuration showing another interim configuration of the structure;

FIG. **4** is a schematic cross-sectional configuration showing the final configuration of the structure;

FIG. **5** is a plan view of the final configuration of the completed edge geometry weak link superconductor of the present invention;

FIG. **6** is a graph of the current-voltage characteristics at 61.5 K of a 50 Å thick weak link barrier of the present invention;

FIG. **7** is a voltage versus wavelength graph of Josephson steps under 10 GHz microwave irradiation;

FIG. **8** is a comparison graph of Jc versus temperature curve for three weak link barrier thicknesses;

FIG. **9** is a graph of the log relationship of current versus temperature for a 50 Å weak link barrier;

FIG. **10** is a graph of Intensity vs Binding Energy for O 1 s spectra;

FIG. **11** is a graph comparison of the second derivatives of the spectra of FIG. **10**;

FIG. **12** is a graph comparison of the valence bands measured at normal emission, and

FIG. **13** is a graph comparison of in (Jc) versus weak link barrier thickness.

DETAILED DESCRIPTION OF THE INVENTION

The following description is provided to enable any person skilled in the art to make and use the invention and sets forth the best modes contemplated by the inventor of carrying out his invention. Various modifications, however, will remain readily apparent to those skilled in the art, since the generic principles of the present invention have been defined herein specifically to provide a method of providing an improved SNS superconductor junction with a weak link barrier.

The present invention seeks to resolve the severe surface problems that have prevented a successful production fabrication of a high quality, high temperature superconducting junction to date by attempting to provide a highly compatible normal metal weak link layer. This goal is sought to be achieved by providing a relatively clean normal metal/superconductor interface with any damaged layers being approximately less than one coherence length ξ thick and the weak link length or thickness being within an effective length relative to the normal metal coherence length with an appropriate submicron layer cross-sectional dimension that will be adequate to achieve device impedances which are high enough to couple to external circuitry.

The present invention is achieved through the growth of an epitaxial YBaCuO/normal-metal/YBaCuO trilayer in either a sandwich or edge geometry configuration. The normal metal barrier layer N----YBaCuO is expected to have a relatively close lattice match to YBaCuO as well as a similar crystal structure so that it will provide a template for overgrowth of a counter-electrode. The thin weak link layer should further be chemically compatible with YBaCuO at the growth temperature and should be able to grow in a two-dimensional fashion with as few pin holes as possible.

The normal metal layer should have a relatively long coherence length and a high resistivity. An advantage of an edge geometry epitaxial tri-layer approach is that it allows a very short weak layer length to be achieved because the effective length is determined by the thickness of the normal metal layer.

The specific embodiments described herein were accomplished with a YBaCuO system which is in the family of rare earth-alkaline earth-cuprate superconductors. It is believed that the advantages of the present invention can be achieved with other ceramic high temperature superconductor systems, as would be expected by a person of skill in this field.

The present invention utilizes a nonsuperconducting Y—Ba—Cu—O (N—YBaCuO) weak link barrier material that is specifically grown at a reduced temperature. The choice of such a weak link barrier material has an obvious advantage of chemical compatibility with the base electrode and counter-electrode to form a high quality $YBa_2Cu_3O_{7-x}$/normal-metal/$YBa_2Cu_3O_{7-x}$ structure. It is believed that the particular choice of our normal metal weak link barrier material will encourage epitaxial overgrowth of the counter-electrode because the lattice constants reported for oxygen-deficient $YBa_2Cu_3O_{7-x}$ and for the possible cubic $YBa_2Cu_3O_{7-x}$ phase are close to those for more fully oxidized $YBa_2Cu_3O_{7-x}$.

The exact structure of the normal metal weak link barrier is not fully known and it is possible that a simple cubic perovskite structure is grown in accordance with the method of the present invention. There is difficulty in obtaining quantitive information on such very thin films grown on a small area and the experiments performed and reported herein suggest that our structure may be cubic. Another possibility is that a metastable, oxygen-rich, nonsuperconducting, tetragonal phase of $YBa_2Cu_3O_{7-x}$ may have been formed under the low temperature processing condition. For purposes of defining the present invention the procedure disclosed is sufficiently operative to reproduce the Josephson element of the present invention.

Recent theoretical results also suggest that higher resistivity materials, such as nonsuperconducting Y—Ba—Cu—O may be more suitable for obtaining high I_cR_n products than low resistivity metals, such as Au or Ag.

In the preferred embodiment and method of the present invention, we have defined a particular junction configuration as an edge geometry weak link, because it is believed in the preferred embodiment that this structure offers some advantages over other possible geometry, such as the sandwich and lateral geometry devices that are known. It should be appreciated, however, that the present invention is not necessarily limited to an edge geometry, although it is believed that this is the preferred embodiment.

The basic device structure of the present invention is formed by depositing the N—YBaCuO layer and the $YBa_2Cu_3O_{7-x}$ layer counter-electrode on the exposed edge of a c-axis-oriented $YBa_2Cu_3O_{7-x}$ thin film overlaid by a thick insulator. The insulator prevents electrical contact to the top surface of the base electrode, so that the active device area is determined by the thickness of the lower $YBa_2Cu_3O_{7-x}$ film and the width of the patterned counter-electrode. This allows very small device areas to be achieved using conventional photolithography. In addition, the effective microbridge length is determined by the thickness of the deposited weak link material so that extremely short bridge lengths are possible, provided that thin, uniform layers can be grown on the $YBa_2Cu_3O_{7-x}$ edge. The edge geometry also has the advantages, that, for c-axis $YBa_2Cu_3O_{7-x}$ films, the current flow in the device active area and lead-in electrodes is along the high current density a-b planes, and that the critical normal-superconductor device interfaces are located on the longer coherence length surfaces perpendicular to the a-b planes.

The growth conditions for the superconducting and nonsuperconducting YBaCuO thin films used in the method of production were nominally identical except for the substrate temperature and the deposition rate. Each of the Y—Ba—Cu—O films were deposited by pulsed excimer laser ablation of a target source at 248 nm and an energy density of approximately 1 J/cm^2. The stoichiometry of our target source was 1:2:3:7 Y:Ba:Cu:O. The oxygen pressure during deposition was within the range of 100 to 200 m Torrs and preferably at 200 m Torrs, and the deposition rate was 1–2 Å/pulse.

The thin weak link N—YBaCuO layer was typically grown at a laser repetition rate of 1 Hz, while the thicker superconducting electrode layers were grown at 5–10 Hz. The backing plate temperature during growth of the nonsuperconducting YBaCuO films was approximately 520–540° C., and about 790–830° C. during growth of the base and counter-electrode superconducting layers. In productionr the YBaCuo weak link barrier deposition was immediately followed by a higher growth temperature for depositing the counter-electrode, and the deposited layers were then annealed in 50–100 Torrs of oxygen at approximately 500° C. for 12 minutes. This annealing procedure was also used after the depositing of the base electrode films. Typical film thicknesses are 25 Å to 100 Å for the N—YBaCuO, and 1500–3000 Å for the superconducting electrodes.

The preferred edge-geometry device fabrication process of the present invention avoids the use of shadow masks in favor of standard integrated circuit processing techniques, which should be readily extendable to more complex circuits. The basic processing steps are briefly outlined here with schematic side and top views of a competed device shown in FIG. **1** through **5**. The fabrication process begins with the deposition of the $YBa_2Cu_3O_{7-x}$ base electrode film on a substrate, such as a properly cleaned and prepared $SrTiO_3$ (100) or $LaAlO_3$ (100) substrate. This is followed by the annealing step. Subsequently, a thick MgO film is patterned by photolithography and liftoff, as shown in FIG. **1**. The MgO layer is utilized as an ion milling mask to define a self-aligned edge in the base electrode using 500 eV Ar ions, followed by a brief 50 eV Ar ion edge cleaning, see FIG. **2**. In some cases, the ion-milling edge cutting process is done at non-normal incidence to produce a more tapered YBaCuO base electrode edge.

Immediately after this step, within the same vacuum system, the substrate temperature is increased and the N—YBaCuO barrier layer **8** and $YBa_2Cu_3O_{7-x}$ counterelectrode **10** are deposited. After annealing, a second lithography and ion milling step is used to cut via holes through the MgO to the base electrode and liftoff Au 12 pads, as shown in FIG. **3**. Finally, a third lithography and ion milling process defines the counter-electrode patterns that can be seen in FIGS. **4** and **5**.

The best results were obtained with edge-geometry weak links having 50 Å thick N—YBaCuO barrier layer at temperatures above 50 K. A typical I-V characteristic at 61.5 K for such a device is shown in FIG. **6**. The I-V curve is qualitatively consistent with the RSJ model, unlike the piecewise-linear or flux-flow characteristics often observed with other all-high T_c weak links. This particular weak link

had a current density of 6.5 kA/cm^2 and an I_cR_n product of 105 μV at this temperature. While at 4.2 K, the I_cR_n products are not as large as theoretically possible, it is believed that larger I_cR_n values may result from improvements in counter-electrode overgrowth. The resistance of this 11 μm×0.28 μm device is ≈0.5 Ω and it is believed that 5 Ω device resistances should be achievable with 1 μm lithography, and 50 Ω with 0.1 μm lithography.

As shown in FIG. **7**, this invention exhibited strong microwave response, with ac Josephson steps at the expected voltages (V_n=nhv/2e) under 10 GHz microwave irradiation. The microwave step amplitudes showed Bessel-function-like oscillatory behavior with increasing RF field, qualitatively consistent with an RSJ current source model. At 4.2 K the 50 Å barrier devices had current densities of about 10^5 A/cm^2, but showed less ideal device characteristics, with flux-flow-type I-V curves and weak microwave response. The non-ideal I-V characteristics in this case may be due to self-shielding effects related to the small Josephson penetration depth (λ_J) in these high J_c, relative wide junctions.

Devices with 25 Å and 100 Å thick N---Ba---Cu---O weak link barrier layers were also tested. At 4.2 K and higher temperatures the weak links with 100 Å barriers sometimes exhibited RSJ-like I-V characteristics, but many of the devices had non-ideal piecewise-linear I-V curves. Some of these devices showed ac Josephson steps which modulated completely with increasing RF power, but typically the magnetic field modulation of the critical currents was less then 30%. The 25 Å barriers devices often showed RSJ I-V characteristics at higher temperatures with strong microwave response up to ~85 K. However, these weak links also showed incomplete (<70%) magnetic field modulation and exhibited hysteresis and switching noise at low voltages, which may be related to switching of weak spots or pin holes in these very thin barriers. In contrast to the 25 and 100 Å barrier devices, above 50 K the 50 Å barrier weak links typically showed 80–100% critical current modulation in applied magnetic fields. The I_c vs B data for such devices exhibited diffraction patterns approximating the expected Fraunhofer behavior, with a strong central peak and periodic I_c modulation, but some asymmetry in the pattern, indicating fairly good barrier uniformity. In these preliminary magnetic field measurements, the field was not applied parallel to the junction base electrode edge, so quantitative determination of the effective device area was not possible.

Another important indicator of the uniformity of the N---YBaCuo barrier layers is the scaling behavior of the critical current and device resistance with barrier thickness and device area. See FIG. **13** for a plot of ln(Jc) as a function of N---YsaCuO normal metal thickness at 4.2 K. The linear data fit indicates that J_c is proportional to $\exp(-L/\xi_n)$, where to ξ_n≈20 Å is the normal metal coherence length. Such exponential scaling of J_c with the normal metal weak link barrier thickness is predicted by simple theories of SNS behavior. The temperature dependence of the critical current density for devices with 25, 50, and 100 Å barrier thicknesses is shown in FIGS. **8** and **9**. The qualitative shape of the J_c vs T curves is similar for all three barrier thicknesses, and a fit of the data for the 50 Å barrier device, see FIG. **9**, indicates that I_c goes as $(1-T/T_c)^2$ near T_c as predicted by basic theories for SNS devices. FIG. **8** clearly shows the strong dependence of critical current on barrier thickness with J_c at 4.2 K ranging from 8.3×10^3 A/cm^2 for the 100 Å barrier, to 3.8×10^5 A/cm^2 for the 25 Å barrier. These devices also show resistances which scale inversely with the device area, and average R_nA products at 4.2 K for the 25, 50, and 100 Å barrier thicknesses are 2.7×10^{-9}, 7.7×10^{-9}, and 1.2×10^{-8} Ω-cm^2, respectively. The scaling of J_c and R_n with barrier thickness and device area indicates that the N---YBaCuO weak link barrier layers are indeed relatively uniform, and that the device behavior is not dominated by pin hole conduction. In contrast to the lateral resistivity measurements of N---YBaCuO films on $LaAlO_3$ substrates, preliminary tests show a factor of 2--3 decrease in device resistance as the temperature is lowered from ≈80 K to 4.2 K. However, the magnitudes of the device R_nA products are consistent with the low end of the resistivity range seen in lateral transport experiments.

In summary, high quality, all-high T_c edge-geometry weak links have been fabricated using nonsuperconducting N---YBaCuO barrier weak link layers in a production process with excellent yields. The best results were obtained with devices incorporating 50 Å barrier layers, which show RSJ-like I-V characteristics with strong ac and dc Josephson effects. The scaling behavior of J_c and R_n with barrier thickness and area indicates that the N---YBaCuO barrier layers form uniform, high quality weak links with an effective normal metal coherence length of 20 Å at 4.2 K.

In an effort to further define the structure of the specific superconducting electrodes and weak link barrier layer, the results of X-ray photoelectron spectroscopy (XPS) measurements are presented.

Each of the film layer specimens were immersed for 30–60 seconds in 1% Br_2 in absolute ethanol, followed by rinsing in ethanol and blow drying with nitrogen. The XPS spectra were accumulated at room temperature on a Surface science Instruments SSX100-501 spectrometer with monochromatized Al K_α X-rays (1486.6 eV) and a base pressure <3×10^{-20} Torrs and a typical operating pressure of 4--6×10^{-10} Torrs. For these experiments, an X-ray spot size of 600 μm and an analyzer pass energy of 25 eV are used, yielding a peak full width at half maximum (FWHM) of 0.7 eV measured for the Au $4f_{7/2}$ peak from an evaporated Au film. For the measurements presented here, the standard sample mount for this spectrometer has been replaced by a custom mount which allowed variable angle measurement. Since the photoelectron energy analyzer has a solid angel of acceptance of 30°, these data should be viewed as angle-integrated measurements centered at the specified angle, rather than as angle-resolved measurements.

The O 1s spectra measured from orthorhombic YBaCuO, Tetragonal YBaCuO, and the N---YBaCuO weak link film were compared in FIG. **10**. All three spectra exhibited peaks at higher binding energy associated with residual nonsuperconducting surface species, which will not be considered here. The lower binding energy peaks in the t-YBaCuO and N---YBaCuO spectra are narrower than that of o-YBaCuO, and the t-YBaCuO peak is shifted to higher binding energy. The o-YBaCuO spectrum had a clear shoulder on the low binding energy side of the main peak and a less obvious shoulder on the high binding energy side which is evident when comparison is made to the N---YBaCuO, which can be fitted with a single peak.

The second derivatives, in which peak positions appear as troughs and weak structure is enhanced, of the spectra from FIG. **10** are shown in the top three curves in FIG. **11**. These data confirm that the t-YBaCuO and N---YBaCuO spectra consist of single peaks at 528.8 eV and 528.1 eV, respectively, and the previously unresolved three peaks comprising the o-YBaCuO spectrum now appear as well-resolved components. The peaks at 527.1 and 528.0 eV are believed to be intrinsic to o-YBaCuO, corresponding to

Cu----O chains and Cu----O planes, respectively. The peak at 528.7 eV is surface related, evident in its enhanced relative intensity at grazing angles (compare the bottom two curves in FIG. **11**). The occurrence of this peak at the same position as that of t-YBaCuO suggests that it may correspond to some residual t-YBaCuO due to incomplete oxidation or oxygen loss at the surface in vacuum. However, no other spectral features associated with t-YBaCuO were observed. As subsequently discussed, a possible origin of this peak is reconstruction of the Cu—O planes which terminate chemically-etched o-YBaCuO surfaces. The absence of this feature and the peak associated with Cu----O chains in the N----YBaCuO may indicate a simple perovskite crystal structure in which Cu----O planes and chains do not exist.

Within experimental error, the Cu 2ρ core level and Cu LMM Auger signals for N----YBaCuO are identical to those for o-YBaCuO. The intensity of the satellite peak in the Cu 2ρ spectrum, characteristic of Cu in the +2 oxidation state was 43% of the intensity of the main peak for both o-YBaCuO and N—YBaCuO, while it is 0.29 for t-YBaCuO, and the Cu^{+1} signal evident in t-YBaCuO is absent in N----YBaCuO. This observation suggests that N—YBaCuO is not simply an oxygen deficient YBaCuO. The other core level signals from N—YBaCuO are also very similar to those from o-YBaCuO. The Y $3d_{5/2}$ is observed at 155.8 eV, 155.9 eV, and 156.4 eV for o-YBaCuO, N—YBaCuO, and t-YBaCuO, respectively, and the corresponding Ba $3d_{5/2}$ ($4d_{5/2}$) peaks were observed at 777.6 eV (87.2 eV), 777.8 eV (87.4 eV) and 778.6 eV (88.2 eV), respectively. The Ba MNN Auger signals from N—YBaCuO and o-YBaCuO are identical within experimental error. These data imply that the potentials at the Y, Ba, and Cu sites may be similar in o-YBaCuO and N----YBaCuO.

The overall shape of the valence band spectrum from N----YBaCuO is similar to that from o-YBaCuO, as shown in FIG. **12**, but is slightly narrower, primarily on the low binding energy side, and with less intensity at the Fermi level. A Fermi edge is evident in the o-YBaCuO spectrum, reflecting the normal state metallic conductivity and providing evidence of a high quality surface. The valence band spectrum from t-YBaCuO differs significantly from the spectra in FIG. **12**, in having negligible intensity at the Fermi level and also significantly different features. The lower intensity in the N—YBaCuO spectrum in the 0–2 eV range is consistent with a lack of Cu 3d-O 2ρ π-bonding states from Cu----O chains, and is thus consistent with expectations from a possible simple perovskite crystal structure.

In summary, XPS characterization of a nonsuperconducting N----YBaCuO SNS weak link barrier material shows that the spectral features are distinct from those of the o-YBaCuO and t-YBaCuO phases, especially in the O 1s region. Features associated with Cu----O chains and surface-reconstructed Cu----O planes are absent in the N----YBaCuO spectra, consistent with a possible, simple perovskite crystal structure.

Those skilled in the art will appreciate that various adaptations and modifications of the just-described preferred embodiments can be configured without departing from the scope and spirit of the invention. Therefore, it is to be understood that, within the scope of the appended claims, the invention may be practiced other than as specifically described herein.

I claim:

1. A method of producing a high temperature superconductor Josephson element comprising the steps of:

providing a substrate;

depositing a lower superconducting electrode film layer of YBaCuO on the substrate;

depositing a weak link barrier layer of a nonsuperconducting film of N—YBaCuO on the lower film layer, and

depositing an upper superconducting counter-electrode film layer of YBaCuO on the barrier layer.

2. The method of claim **1** wherein the lower superconducting film layer has an exposed edge of a c-axis oriented $YBa_2Cu_3O_{7-x}$ film layer and the weak link barrier layer of nonsuperconducting film is deposited over the exposed edge.

3. The method of claim **1** wherein the lower electrode superconducting film and upper electrode superconducting film are deposited at approximately a temperature range of 790° C. to 830° C. and the nonsuperconducting film is deposited at a temperature range of 520° C. to 540° C. in 100 to 200 m Torrs of oxygen.

4. The method of claim **1** wherein the weak link barrier layer is deposited to form a layer thickness within a range of 25 Å to 100 Å.

5. The method of claim **1** wherein the respective lower and upper superconducting film layers are deposited to form film thicknesses within the range of 1000 Å to 3500 Å.

6. The method of claim **1** wherein the formation of the respective layers occurred in a deposition step with an oxygen pressure of 100 to 200 m Torrs.

7. The method of claim **1** wherein the formation of the respective film layers occurred by exposing a $YBa_2Cu_3O_{7-x}$ target to a pulsed excimer laser at 248 mm and an energy density of 1 to 2 J/cm^2.

8. The method of claim **7** wherein the formation of the respective film layers occurred by depositing the lower and upper superconducting film layer at a deposition rate of approximately 1–2 Å/pulse at a pulse rate of 5–10 Hz and the barrier layer at a deposition rate of approximately 1–2 Å/pulse rate of 1 Hz.

9. The method of claim **8** wherein the weak link barrier layer has a thickness of approximately 5 Å to 200 Å.

10. The method of claim **1** wherein the weak link barrier layer is deposited to form a layer thickness of 50 Å.

11. The method of claim **1** further including the step of providing a clean normal metal/superconductor interface between said lower layer and said barrier layer with any damage to said lower layer being approximately less than one coherence length thick.

12. A method of producing a high temperature superconductor Josephson junction comprising the steps of:

providing a substrate;

depositing a lower superconducting electrode film layer of YBaCuO on the substrate;

depositing a weak link barrier layer of a nonsuperconducting film of N----YBaCuO on the lower film layer to form a layer having a thickness within a range of 5 Å to 200 Å; and

depositing an upper superconducting counter-electrode film layer of YbaCuO on the barrier layer;

wherein the lower electrode superconducting film and upper electrode superconducting film are deposited at a temperature range of 790° C. to 830° C. and the nonsuperconducting barrier layer is deposited at a temperature range of 520°; to 540° C.;

wherein the formation of each of the respective lower, barrier, and upper layers occurs in a deposition step with an oxygen pressure of 100 to 200 m Torrs; and

wherein the formation of the respective upper, lower, and barrier film layers is achieved by exposing a

$YBa_2Cu_3O_{7-x}$ target to a pulsed excimer laser and depositing the lower and upper superconducting films layer at a deposition rate of approximately 1–2 Å/pulse at a pulse rate of 5–10 Hz and the barrier layer at a deposition rate of approximately 1–2 Å/pulse at a pulse rate of 1 Hz.

13. The method of claim **12** wherein the thickness of the weak link barrier is 50 Å.

14. The method of claim **12** further including the step of providing a clean normal metal/superconductor interface between said lower layer and said barrier layer with any damage to said lower layer being approximately less than one coherence length thick.

15. The method of claim **12** wherein the lower superconducting film layer has an exposed edge of a c-axis oriented $YBa_2Cu_3O_{7-x}$ film layer and the weak link barrier layer of nonsuperconducting film is deposited over the exposed edge.

16. A method of producing a high temperature superconductor Josephson junction comprising the steps of:

providing a substrate;

depositing a lower superconducting electrode film layer of YBaCuO on the substrate;

depositing a weak link barrier layer comprising a nonsuperconducting film of N—YBaCuO on the lower film layer; and

depositing an upper superconducting counter-electrode film layer of YBaCuO on the barrier layer.

17. The method of claim **16** wherein the lower electrode superconducting film and upper electrode superconducting film are deposited at approximately a temperature range of 790° C. to 830° C. and the nonsuperconducting film is deposited at a temperature range of 520° C. to 540° C. in 100 to 200 m Torrs of oxygen.

18. The method of claim **17** wherein the weak link barrier layer is deposited to form a layer thickness of 50 Å.

19. A method of producing a SNS high temperature superconductor Josephson junction comprising the steps of:

providing a substrate;

depositing a lower superconducting electrode film layer of YBaCuO on the substrate;

depositing a weak link barrier layer comprising a nonsuperconducting film of YBaCuO on the lower film layer; and

depositing an upper superconducting counter-electrode film layer of YBaCuO on the barrier layer.

20. The method of claim **19** wherein the lower electrode superconducting film and upper electrode superconducting film are deposited at approximately a temperature range of 790° C. to 830° C. and the nonsuperconducting film is deposited at a temperature range of 520° C. to 540° C. in 100 to 200 m Torrs of oxygen.

21. The method of claim **20** wherein the weak link barrier layer is deposited to form a layer thickness of 50 Å.

22. The method of claim **17** wherein the formation of the upper and lower superconducting films occurs in a deposition step with an oxygen pressure of 100 to 200 m Torrs.

23. The method of claim **20** wherein the formation of the upper and lower superconducting films occurs in a deposition step with an oxygen pressure of 100 to 200 m Torrs.

24. The method of claim **22** wherein the Y—Ba—Cu—O barrier deposition is immediately followed by a ramp to the higher growth temperature, the counter-electrode is then deposited, and the upper, lower and barrier layers are then annealed in 50 Torrs of oxygen at 500° C. for 12 minutes.

25. The method of claim **23** wherein the Y—Ba—Cu—O barrier deposition is immediately followed by a ramp to the higher growth temperature, the counter-electrode is then deposited, and the upper, lower and barrier layers are then annealed in 50 Torrs of oxygen at ≈500° C. for 12 minutes.

26. The method of claim **22** wherein the lower superconducting film layer has an exposed edge of a c-axis oriented $YBa_2Cu_3O_{7-x}$ film layer and the weak link barrier layer of nonsuperconducting film is deposited over the exposed edge.

27. The method of claim **23** wherein the lower superconducting film layer has an exposed edge of a c-axis oriented $YBa_2Cu_3O_{7-x}$ film layer and the weak link barrier layer of nonsuperconducting film is deposited over the exposed edge.

* * * * *

USSN 10/751,091

EVIDENCE APPENDIX

ATTACHMENT B.3

USSN 10/751,091

EVIDENCE APPENDIX

ATTACHMENT B.3

ECS Vol 93-22
pp 462-472

Invited paper at the Second Symposium on Low Temperature Electronics and High Temperature Superconductivity, Electrochemical Society Meeting, Honolulu, Hawaii, May 17-21, 1993

HIGH TEMPERATURE SUPERCONDUCTOR JOSEPHSON WEAK LINKS

B. D. Hunt, J. B. Barner, M. C. Foote, and R. P. Vasquez
Center for Space Microelectronics Technology, Jet Propulsion Laboratory,
California Institute of Technology, Pasadena, CA 91109

High T_c edge-geometry SNS microbridges have been fabricated using ion-damaged $YBa_2Cu_3O_{7-x}$ (YBCO) and a nonsuperconducting phase of YBCO (N-YBCO) as normal metals. Optimization of the ion milling process used for YBCO edge formation and cleaning has resulted in ion-damage barrier devices which exhibit I-V characteristics consistent with the Resistively-Shunted-Junction (RSJ) model, with typical current densities (J_c) of $\approx 5 \times 10^6$ A/cm^2 at 4.2 K. Characterization of N-YBCO films suggests that N-YBCO is the orthorhombic YBCO phase with oxygen disorder suppressing T_c. Weak links using N-YBCO as the normal metal show RSJ I-V characteristics and exponential scaling of J_c, with a normal metal coherence length of $\approx$ 23 Å. In behavior similar to that reported for grain boundary junctions, the N-YBCO I_cR_n products scale as $J_c^{0.84}$ for current densities below 10^5 A/cm^2. For both types of devices, typical I_cR_n products at 4.2 K are limited to 1 - 2 mV at the highest current densities, possibly due to self-shielding effects.

INTRODUCTION

High temperature superconductor (HTS) Josephson devices are potentially useful for a variety of applications including high speed digital logic, Thz frequency sources and detectors, and sensitive magnetometers. One promising approach to HTS Josephson device fabrication is the use of superconductor/normal-metal/superconductor (SNS) microbridges. Such weak links generally possess nonhysteretic current-voltage (I-V) characteristics, which are well-suited for high speed logic and magnetometer applications. In addition, the utilization of a normal metal bridge can relax the severe bridge length constraints of an all-superconducting microbridge. This approach also allows control of J_c and R_n over a broad range simply by varying the normal metal bridge length.

There are a number of possible device geometries for fabrication of HTS SNS weak links including planar SNS microbridges (1,2,3,4), step-edge SNS weak links (5,6,7), sandwich-geometry SNS trilayers (8,9,10,11,12), and edge-geometry SNS weak links (13,14,15,16,17,18,19,20). This work focuses on epitaxial edge-geometry SNS weak links due to advantages associated with this approach. A schematic diagram of an edge geometry SNS weak link is shown in Figure 1. The basic device structure consists of a c-axis-oriented YBCO base electrode with an exposed edge. An epitaxial normal metal is deposited on the YBCO edge, followed by deposition of the YBCO counterelectrode. Because the top surface of the base electrode is covered by a thick insulator, electrical contact between the YBCO electrodes is confined to the edge of the lower YBCO film.

The principal advantages of the edge geometry include the facts that the critical N/S interfaces are located on the longer coherence length YBCO surfaces, current flow is along the high J_c direction parallel to the a-b planes throughout the device, and very small device areas can be produced using conventional photolithography. The edge geometry also enables very short microbridge lengths to be achieved and controlled, because the bridge length is determined by the deposited normal metal thickness. Edge junction

fabrication is somewhat simpler than for trilayer SNS devices, because the counter-electrode serves as the wiring layer and no additional insulator and wiring depositions are needed. A possible drawback of the edge geometry approach is that the ion milling process used to define the base electrode edge may cause YBCO surface damage. In addition, optimal device performance requires formation of tapered YBCO edges (discussed below). Because typical tapered edge fabrication processes produce YBCO edges with a single orientation, circuit layout can be more complex with these devices.

One of the most important factors in determining high T_c SNS device performance is the choice of which normal metal to incorporate in the device structure. In an all-epitaxial weak link, the normal metal must be lattice-matched to YBCO in order to provide a template for overgrowth of the counterelectrode. Two very important, but difficult requirements are that the normal metal be chemically compatible with YBCO at the counterelectrode growth temperature, and that the normal metal film should grow without thin spots or pinholes. A long normal metal coherence length is also desirable, and theoretical arguments suggest that the normal metal resistivity-coherence length product ($\rho_n\xi_n$) should be larger than the corresponding product for YBCO (21). These requirements severely restrict possible normal metal choices for HTS epitaxial weak links. This work examines new results with two different weak link barrier layers that meet at least some of the above constraints: ion-damaged YBCO layers and a nonsuperconducting phase of YBCO (15,16). Special attention is paid to optimization of the edge formation and edge cleaning processes, which are closely related to the ion-damaged weak links. The primary goals of this work were to develop a reliable and reproducible HTS device process, and to obtain improved HTS SNS device performance. As will be seen below, good results have been achieved using both weak link materials. However, additional improvements are still needed for some device applications, and strategies for further optimization will be discussed.

DEVICE FABRICATION

Details of the edge-geometry weak link fabrication process have been described previously (15,16,18,22), but will be briefly summarized here. Device fabrication begins with pulsed laser deposition of a c-axis-oriented YBCO thin film, typically on a $LaAlO_3$ substrate. Following growth of the base electrode, a thin (100-200 Å) MgO or cubic zirconia passivation layer is deposited over the YBCO before removal from the laser ablation chamber. Next a thick (6000-9000 Å) MgO layer is patterned using photolithography and liftoff. The patterned MgO film is utilized as an ion milling mask to produce a tapered edge in the YBCO base electrode, followed by a low energy ion cleaning step. This edge formation process is discussed in greater detail below. Just after cleaning of the YBCO edge, within the same vacuum system, the normal metal layer and YBCO counterelectrode are deposited at the appropriate growth temperatures. A lithography-ion milling step is then used to pattern via holes down to the base YBCO film and liftoff Au contact pads. Finally, another lithography-milling process defines the counterelectrode. Completed devices have counterelectrode widths ranging from 6 μm down to 1.5 μm.

EDGE CLEANING OPTIMIZATION AND ION-DAMAGED-YBCO WEAK LINKS

One of the most critical steps of edge-geometry weak link fabrication is the YBCO edge formation and cleaning process. The two key requirements for formation of the YBCO edge are: 1) that the edge must be tapered to prevent grain boundary formation in

the YBCO counterelectrode (23), and 2) that surface damage on the YBCO base electrode surface is minimized. Tapered YBCO edges are produced by Ar ion milling at an approximately 30° angle from the substrate surface (16). This angled ion milling edge cutting step is followed by a low energy ion cleaning step at normal incidence to the substrate surface. Both the edge cutting and edge cleaning steps are done in a turbo-pumped load-lock attached to the main laser ablation chamber. Between these two steps the device chip is transferred from one fixture to another inside the vented load lock under flowing N_2 gas, so that any air-exposure is minimal.

It is important to minimize ion surface damage on the YBCO base electrode edge, because such damage can result in a suppression of the energy gap in the YBCO film at the YBCO-normal metal interface, leading to a reduction of the device I_cR_n product. Edge surface damage may also result in a degradation of the quality of epitaxial overgrowth of the normal metal and counterelectrode layers. The degraded layer on the YBCO base electrode is caused by ion damage during the edge cutting and edge cleaning steps, and presumably consists of both crystalline defects and stoichiometry shifts associated with preferential ion sputtering. Shifts in oxygen stoichiometry due to oxygen loss and oxygen disorder may be especially serious problems at the YBCO-normal metal interface due to the relatively high mobility of oxygen in YBCO (24). The thickness of the YBCO damage layer is related to the energy of the impinging ions and their angle of incidence. However, it is probably not correct to simply equate the damage layer thickness with the incident ion range, because some damage may anneal out during heating in oxygen for the counterelectrode growth, and also because oxygen disordering may extend deeper than the primary ion damage depth.

In order to investigate the effect of edge ion milling and cleaning parameters, we have examined the electrical properties of devices produced with no deposited normal metal layer, where the counterelectrode is deposited directly on the ion-milled YBCO base electrode edge. These experiments were done in an effort to optimize the edge junction cleaning procedure for application to devices with deposited normal metals, and also to investigate whether high quality, controllable weak links could be produced using an ion-damaged YBCO surface layer as a "normal metal". In fact, some of the first devices fabricated without deposited normal metal layers showed excellent electrical performance, as shown in the 77 K I-V characteristics of Figure 2(a). For this weak link, the YBCO edge was produced by Ar-ion-milling at 500 eV at 30° from the substrate surface, followed by a 50 eV normal incidence Ar ion cleaning step. This device has a current density of $\approx 5 \times 10^4$ A/cm^2 at 77 K with an I_cR_n product of 153 μV and an R_nA product of 2.9×10^{-9} Ω-cm^2. The I-V characteristics are qualitatively consistent with the Resistively-Shunted-Junction (RSJ) model, although the devices on this chip do typically exhibit excess currents. The microwave response of this device is shown in Figure 2(b). Clean ac Josephson steps are seen in response to 14.4 GHz microwave irradiation with amplitudes that modulate as expected with increasing microwave power. These initial results encouraged us to investigate ion-damaged barrier weak links in more detail to see whether reproducible and controllable weak links could be produced in this manner.

As part of this study, a set of ion-damage barrier chips was fabricated using 500 eV Ar ions to etch tapered YBCO edges, followed by a normal-incidence Ar ion clean at ion energies ranging from 50 to 500 eV. The weak link electrical parameters J_c, I_cR_n, and R_nA were measured as a function of Ar ion cleaning energy. For these experiments the cleaning times were adjusted so that at each ion energy, the same total areal dose of 1.9×10^{17} ions/cm^2 was used. Figure 3 shows the dependence of the average value of J_c

on ion beam cleaning energy for four different device chips. The data shows a decrease in J_c with increasing cleaning energy up to 250 eV, as might be expected if the damage depth scales with ion range in the YBCO. However, at 500 eV, the average current density increases to a value close to that seen for the 50 eV cleaning case. This effect is not understood at this time. One point to note is that, although some variation is seen in J_c as the cleaning energy is varied, the total variation in J_c is not large. The other notable fact here is that the devices of Figure 3 exhibited RSJ-like I-V characteristics and ac Josephson steps only for cleaning energies less than or equal to 250 eV. Devices on the chip fabricated using 500 eV Ar ion cleaning showed flux-flow I-V characteristics at all temperatures and no ac Josephson steps under microwave irradiation. The lack of Josephson behavior in the 500 eV-cleaned devices probably indicates that the ion damage depth exceeds the superconducting coherence length.

The dependence of I_cR_n on the ion cleaning energy at 77 K is shown in Figure 4. The average I_cR_n products are roughly independent of cleaning energy below 250 eV, but drop off at the highest cleaning energy. The average I_cR_n values are ≈ 250 μV for the lower cleaning energies, but range up to ≈ 450 μV for some devices. These I_cR_n products are some of the highest reported for SNS weak links at 77 K. The average R_nA products for these chips were lowest for the 50 eV and 500 eV cleans, and highest at 250 eV, ranging from 3×10^{-10} to 1.7×10^{-9} Ω-cm^2 at 77 K. Overall, the best device and cleaning results were obtained using 50 eV Ar cleaning in combination with the 500 eV Ar edge milling step. At 4.2 K, under these conditions, for four chips (30 devices) the average J_c was 5.5×10^6 A/cm^2 with a standard deviation of 4.7×10^6 A/cm^2, the average R_nA product was 5.4×10^{-10} Ω-cm^2 with a standard deviation of 6.4×10^{-10} Ω-cm^2, and the average I_cR_n product was 1.03 mV with a standard deviation of 0.24 mV. Possible self-shielding limitations on I_cR_n are discussed in the next section. Other variations in the YBCO edge formation and cleaning process were also examined, including xenon cleaning, eliminating the ion cleaning step, and varying the edge ion mill etching energy. These process variations produced devices with parameters comparable to the weak links made using 500 eV Ar edge cutting and 50 eV Ar cleaning.

The basic conclusions of the edge formation studies are relevant to YBCO edge cleaning for application to SNS devices with deposited normal metals, as well as to fabrication of ion-damaged-YBCO SNS devices. From a cleaning perspective, the high current densities and low R_nA products found with the 50 eV Ar process indicate that this process produces very clean YBCO edges that should work well as growth templates for epitaxial normal metal devices. However, we do believe that further cleaning optimization should be possible, for example, by going to an entirely *in-situ* cleaning process. This edge formation process has also produced high quality HTS Josephson devices with ion-damaged YBCO layers serving as effective normal metal weak links. These ion-damage barrier devices have high current densities and I_cR_n products at 77 K, making them well-suited for superconducting device applications such as flux-quantum logic and SQUID magnetometers. However, this approach does have some potential drawbacks. The critical current densities of the ion-damage weak links appear to be relatively insensitive to ion cleaning energy and ion species, indicating that J_c in these devices is not controllable over a wide range. This is a problem for some cases in which control of J_c is required, such as integrated circuit applications. In some other situations, however, the insensitivity of J_c to process variations could be a significant advantage. A second potential problem is that the device current densities are approaching the electrode J_c values, which can cause difficulties with electrode transitions unless care is taken to use thick counterelectrodes. Finally, the R_nA products of the ion-damaged barrier weak

links are small, $R_nA \approx 5 \times 10^{-10}$ Ω-cm^2 at 4.2 K, so that 0.1 μm lithography will be required to produce 5 Ω devices.

N-YBCO WEAK LINKS

The edge formation and cleaning process just described provides the basis for fabrication of HTS weak links using deposited epitaxial normal metals. One possible SNS device technology uses a nonsuperconducting phase of $YBa_2Cu_3O_{7-x}$ (N-YBCO) as the normal metal. Some results on fabrication and testing of N-YBCO weak links have been presented previously (15,16). Here we examine new data on N-YBCO characterization and N-YBCO device results, including the scaling behavior of the weak link critical current densities and I_cR_n products.

The N-YBCO thin films are deposited using a standard laser ablation process and a nearly stoichiometric $YBa_2Cu_3O_{7-x}$ target, except that the films are grown at $\approx$ 530 C, a much lower temperature than typically used to produce high quality superconducting YBCO thin films. Because of the difficulty of characterizing N-YBCO films deposited on the very small area YBCO base electrode edge, characterization of these films has been done primarily on N-YBCO layers grown directly on $LaAlO_3$ substrates, followed by a 1-2 minute anneal at $\approx$ 800 C, to mimic the counterelectrode growth conditions. Lateral transport resistivity measurements on 100 Å N-YBCO thin films grown in this manner show semiconductor-like behavior, although in some cases a drop in resistance is seen near 4 K. Resistivity measurements on much thicker N-YBCO films (3000 Å) show a superconducting transition at $\approx$ 40 K. X-ray diffraction studies of 500 - 1000 Å thick N-YBCO show peaks consistent with orthorhombic $YBa_2Cu_3O_{7-x}$ with a c-axis lattice constant of 11.68 Å. X-ray photoelectron spectroscopy (XPS) measurements on N-YBCO films produced with the above annealing procedure show no obvious difference from standard orthorhombic $YBa_2Cu_3O_{7-x}$. Finally, preliminary high resolution cross-sectional transmission electron microscopy (HRTEM) studies give images consistent with an orthorhombic YBCO phase.

These measurements demonstrate that N-YBCO is not the semiconducting cubic phase of YBCO reported by Agostinelli et al. (25). The characterization studies also indicate that N-YBCO is probably not the the nonsuperconducting oxygen-rich (26) or oxygen-poor (27) tetragonal phases reported earlier, because these phases exhibit c-axis lattice parameters smaller or larger than the value of 11.68 Å measured from the x-ray diffraction data. It appears most likely that N-YBCO is orthorhombic $YBa_2Cu_3O_{7-x}$ with oxygen disorder suppressing the transition temperature. A number of studies have shown that YBCO is especially susceptible to oxygen movement and that oxygen disorder can significantly affect T_c (24,28,29). Presumably, crystallization of the low-temperature-deposited YBCO film occurs during the heating ramp to the counterelectrode growth temperature, but sufficient oxygen disorder, and possibly other point defects remain to suppress superconductivity in these films. This supposition is consistent with device results indicating that SNS coupling through N-YBCO is sensitive to the high temperature counterelectrode growth parameters. In particular, we find that weak link current densities increase for hotter counterelectrode growth temperatures. These results suggest that N-YBCO is metastable, and that increased high temperature annealing results in reduced crystalline disorder and stronger weak link coupling. At room temperature, however, the N-YBCO devices are very stable, with almost no change in the current-voltage characteristics after more than a year of storage in an Ar-filled desiccator.

As reported previously (15,16), SNS weak links fabricated with N-YBCO normal metal layers typically exhibit RSJ-like current-voltage characteristics with some excess current. These devices show clean ac Josephson steps at 14.4 GHz, which modulate as expected with increasing microwave power. Studies of the magnetic field dependence of the critical currents in N-YBCO SNS weak links show Fraunhofer-like patterns with 30 - 90% modulation (16). This magnetic field behavior demonstrates good large scale barrier uniformity, but the incomplete modulation is consistent with fine scale nonuniformities in the N-YBCO or the N-S interfaces. Figure 5 is a plot of the average SNS weak link current density for the devices on 25 chips at 4.2 K as a function of the N-YBCO barrier thickness. The straight line is a fit to the data for N-YBCO thicknesses less than or equal to 100 Å, showing that J_c scales exponentially with barrier thickness in this range, with an effective normal metal coherence length of 23 Å. Devices with N-YBCO layers thicker than ≈ 100 Å suffer from degraded counterelectrode quality with lower transition temperatures and higher resistivities. For these devices, a more rapid decrease in J_c with increasing barrier thickness is seen due to the degradation of the counterelectrode properties. This deterioration in the quality of the YBCO counterelectrode suggests that there is an epitaxial growth problem on N-YBCO barriers over 100 Å, presumably because these layers are not providing a good epitaxial growth template for counterelectrode overgrowth. This problem may be eliminated by more careful optimization of the N-YBCO growth and annealing conditions.

Another potential problem with these devices is the variation in device properties. Critical current density standard deviations across a single quarter inch chip were as small as 18%, and typically ranged from 20 - 100%. However, as much as an order of magnitude variation in critical currents was seen from chip to chip for a given barrier thickness, and the J_c standard deviations for all devices from all chips at each N-YBCO thickness ranged from ≈ 70% to 200%. Some of this variability can be attributed to process variations which were investigated during various device fabrication runs. In addition, the short coherence length and metastable nature of N-YBCO make these weak links especially susceptible to planned or unplanned process changes. Tighter process control is expected to help improve reproducibility.

We have also examined the scaling behavior of I_cR_n as a function of J_c for both the N-YBCO and ion-damage barrier devices, as shown in Figure 6. A fit to the data for $J_c < 10^5$ A/cm^2 indicates that I_cR_n scales as $J_c^{0.84}$ over a wide range of current densities. This scaling behavior is similar to that reported for grain boundary weak links and is evidence that transport in these devices occurs through superconducting filaments shunted by normal regions (24). Such nonuniform conduction could result from oxygen disorder in the N-YBCO layers or in the ion-damaged surface layer on the YBCO base electrode. This superconducting filament model is consistent with the magnetic field modulation studies of the critical currents, which pointed to fine scale nonuniformities in these devices. The second important point to note about the data of Figure 6 is that the I_cR_n products for most devices saturate at ≈ 1-2 mV above 10^5 A/cm^2. This effect is probably due to self-shielding effects in these very high J_c devices: we calculate a Josephson penetration depth of ≈ 1 μm at 10^5 A/cm^2 and our minimum device width is 1.5 μm. In fact, a replotting of the data (not shown) indicates that the smaller devices do have higher I_cR_n products at the highest current densities. We plan to fabricate smaller devices using electron beam lithography in an attempt to reproducibly obtain higher I_cR_n products. In addition, we are also examining other epitaxial normal metal layers such as $PrBa_2Cu_3O_{7-x}$ (18) in order to achieve improved weak link reproducibility and higher I_cR_n products at lower current densities.

SUMMARY

We have fabricated and tested HTS edge-geometry weak links utilizing ion-damaged YBCO and a nonsuperconducting phase of YBCO (N-YBCO) as weak link barrier materials. Special attention was focused on optimization of the YBCO base electrode edge formation and cleaning process. It was found that high quality YBCO edges could be prepared using a 500 eV Ar edge milling step in combination with 50 eV Ar cleaning. When used to fabricate weak links with no deposited barrier layer, in which the remnant ion damage serves as the weak link barrier, this cleaning process produced devices with average values of $J_c = 5.5 \times 10^6$ A/cm^2 and average R_nA products of 5.4×10^{-10} Ω-cm^2. The ion-damaged weak links exhibited good quality RSJ I-V characteristics, but could only be fabricated over a relatively limited current density range approaching the YBCO electrode J_c values. We have also produced SNS weak links using N-YBCO layers as the normal metal barrier. Characterization of the N-YBCO films suggests that this material is the orthorhombic phase of $YBa_2Cu_3O_{7-x}$ with oxygen disorder and possibly other point defects suppressing T_c. The N-YBCO weak links show RSJ I-V characteristics with strong microwave and magnetic field response. The critical currents of the N-YBCO devices scale exponentially with barrier thickness for barriers less than 100 Å with a nominal coherence length of 23 Å. The I_cR_n products of these devices are usually limited to 1 - 2 mV, and scale as $J_c^{0.84}$ in behavior similar to that reported for grain boundary junctions, suggesting that transport may be dominated by superconducting filaments shunted by normal regions. The I_cR_n scaling behavior also indicates that higher I_cR_n products may be obtained by fabricating smaller devices at the highest current densities.

AKNOWLEDGEMENTS

The research described in this paper was performed at the Center for Space Microelectronics Technology, Jet Propulsion Laboratory, California Institute of Technology, and was jointly sponsored by the Defense Advanced Research Projects Agency, the Strategic Defense Initiative Organization, Innovative Science and Technology Office, and the National Aeronautics and Space Administration, Office of Advanced Concepts and Technology.

REFERENCES

1. D.B. Schwartz, P.M. Mankiewich, R.E. Howard, L.D. Jackel, B.L. Straughn, E.G. Burkhart, and A.H. Dayem, IEEE Trans. Magnetics 25, 1298 (1989).
2. M.G. Forrester, J. Talvacchio, J.R. Gavaler, M. Rooks, and J. Lindquist, IEEE Trans. Magnetics 27, 3098 (1991).
3. M.S. Wire, R.W. Simon, J.A. Luine, K.P. Daly, S.B. Coons, A.E. Lee, R. Hu, J.F. Burch, and C.E. Platt, IEEE Trans. Magnetics 27, 3106 (1991).
4. B Ghyselen, R. Cabanel, S. Tyc, D.G. Crete, Z.H. Barber, J.E. Evetts, G. Ben Assayag, J. Gierak, and A. Schuhl, Physica C 198, 215 (1992).
5. M.S. Dilorio, S. Yoshizumi, K-Y. Yang, M. Maung, J. Zhang, and B. Power, IEEE Trans. Applied Superconductivity 3, 2011 (1993).
6. R.H. Ono, L.R. Vale, K.R. Kimminau, J.A. Beall, M.W. Cromar, C.D. Reintsema, T.E. Harvey, P.A. Rosenthal, and D.A. Rudman, IEEE Trans. Applied Superconductivity 3, 2389 (1993).
7. P.A. Rosenthal, E.N. Grossman, R.H. Ono, and L.R. Vale, submitted to Applied Physics Letters (1993).

8. C.T. Rogers, A. Inam, M.S. Hegde, B. Dutta, X.D. Wu, and T. Venkatesan, Appl. Phys. Lett. 55, 2032 (1989).
9. J.B. Barner, C.T. Rogers, A. Inam, R. Ramesh, and S. Bersey, Appl. Phys. Lett. 59, 742 (1991).
10. K. Mizuno, K. Higashino, K. Setsune, and K. Wasa, Appl. Phys. Lett. 56, 1469 (1990).
11. G.F. Virshup, M.E. Klausmeier-Brown, I. Bozovic, and J.N. Eckstein, Appl. Phys. Lett. 60, 2288 (1992).
12. T. Satoh, J. Fujita, T. Yoshitake, and H. Tsuge, Appl. Phys. Lett. 62, 1685 (1993).
13. R.B. Laibowitz, R.H. Koch, A. Gupta, G. Koren, W.J. Gallagher, V. Foglietti, B. Oh, and J.M.Viggiano, Appl. Phys. Lett. 56, 686 (1990).
14. G. Koren, E. Aharoni, E. Polturak, and D. Cohen, Appl. Phys. Lett. 58, 634 (1991).
15. B.D. Hunt, M.C. Foote, and L.J. Bajuk, Appl. Phys. Lett. 59, 982 (1991).
16. B.D.Hunt, L.J.Bajuk, J.B.Barner, M.C. Foote, B.B.Jones, and R.P.Vasquez, SPIE Proceedings Vol. 1597: Progress in High Tc Superconducting Transistors and Other Devices II, 108 (1991).
17. Yu.M. Boguslavskij, J. Gao, A.J. Rijnders, D. Terpstra, G.J. Gerritsma, and H. Rogalla, Physica C 194, 268 (1992).
18. J. B. Barner, B. D. Hunt, W. T. Pike, M. C. Foote, and R. P. Vasquez, Physica C 207, 381 (1993).
19. K.Char, M.S.Colclough, T.H.Geballe, K.E.Myers, Appl. Phys. Lett. 62, 196 (1993).
20. J.A. Agostinelli, J.M. Chwalek, C.J. Baron, G. Lubberts, and C.D. Dowell, Physica C 207, 203 (1993).
21. M.Y. Kupriyanov and K.K. Likharev, IEEE Trans. Magnetics 27, 2460 (1991).
22. M.C. Foote, B.B. Jones, B.D. Hunt, J.B. Barner, R.P. Vasquez and L.J. Bajuk, Physica C 201, 176 (10/92).
23. C.L.Jia, B. Kabius, K. Urban, K. Herrman, G.J. Cui, J. Schubert, W. Zander, and A.I. Braginski, Physica C 175, 545 (1991).
24. B.H. Moeckly, D.K. Lathrop, and R.A. Buhrman, Phys. Rev. B 47, 400 (1993).
25. J.A. Agostinelli, S. Chen, and G. Braunstein, Phys. Rev. B 43, 11396 (1991).
26. K.W. Lay, J. Am. Ceramics Soc. 72, 696 (1989).
27. J.D. Jorgensen, B.W. Veal, A.P. Paulikas, L.J. Nowicki, G.W. Crabtree, H. Claus, and W.K. Kwok, Phys. Rev. B 41, 1863 (1990).
28. B.W.Veal, A.P.Paulikas, H.You, H.Shi, Y.Fang, J.W.Downey, Phys.Rev. B42, 6305.
29. R.J. Cava, A.W. Hewat, E.A. Hewat, B. Batlogg, M. Marezio, K.M. Rabe, J.J. Krajewski, W.F. Peck Jr., and L.W. Rupp Jr., Physica C 165, 419 (1990).

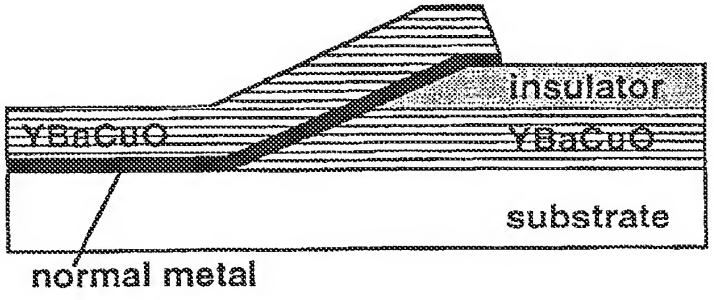

Figure 1. Cross-sectional schematic diagram of edge-geometry SNS weak link.

(a)

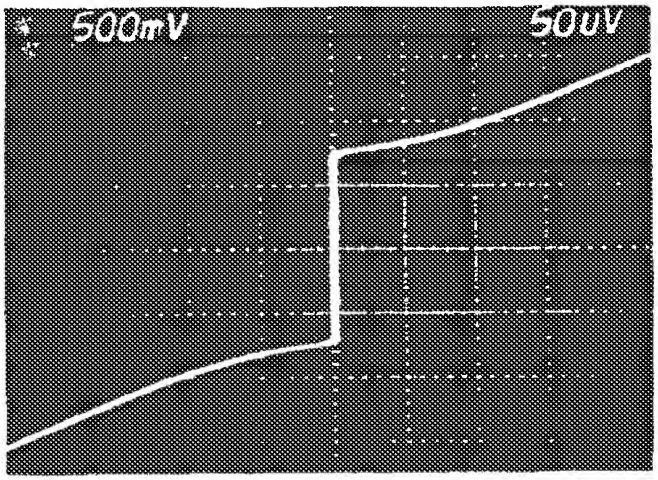

(b)

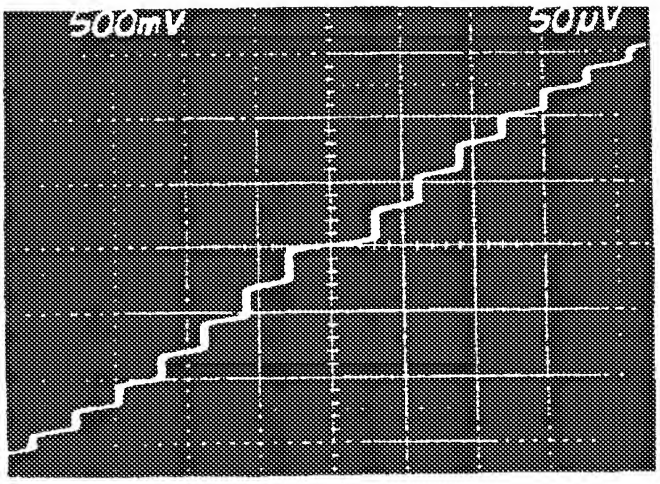

Figure 2. (a) Current-voltage characteristics at 77 K of ion-damaged YBCO weak link produced by Ar-ion milling at 500 eV, and cleaned *in-situ* with 50 eV Ar ions. The device size is 3 μm x 0.46 μm, $J_c = 5 \times 10^4$ A/cm^2, $I_cR_n = 153$ μV, and $R_nA = 2.9 \times 10^{-9}$ Ω-cm^2. (b) Microwave response of ion-damage weak link at 14.4 GHz. For both I-Vs the vertical scale is 0.5 mA/div. and the horizontal scale is 50 μV/div.

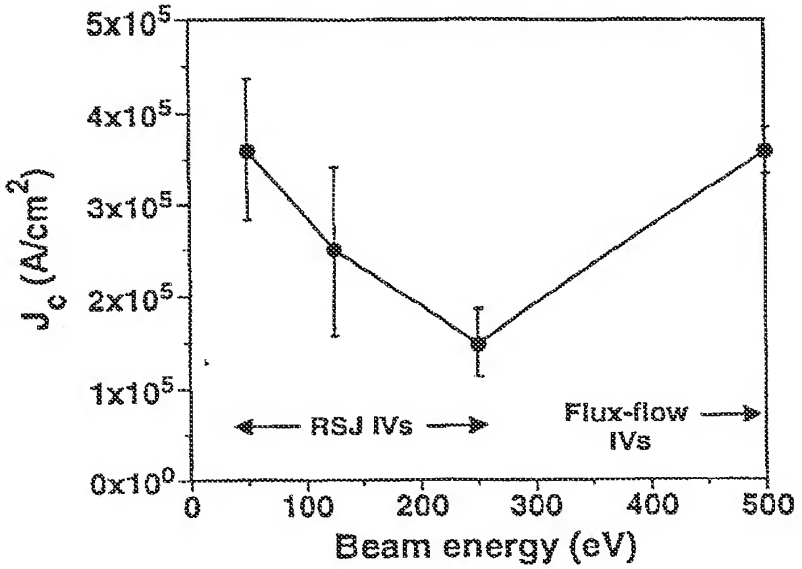

Figure 3. Plot of the average J_c versus Ar cleaning energy at 77 K for weak links on four chips produced with a 500 eV Ar edge cutting process and no deposited barrier layer. The error bars give the standard deviation in J_c for each chip.

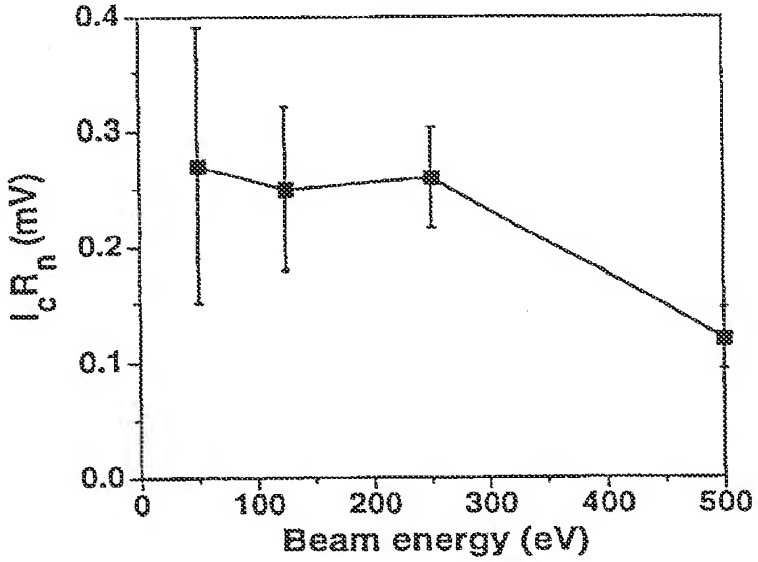

Figure 4. Plot of the average I_cR_n product versus Ar cleaning energy at 77 K for weak links on four chips produced with a 500 eV Ar edge cutting process and no deposited barrier layer. The error bars give the standard deviation in I_cR_n for each chip.

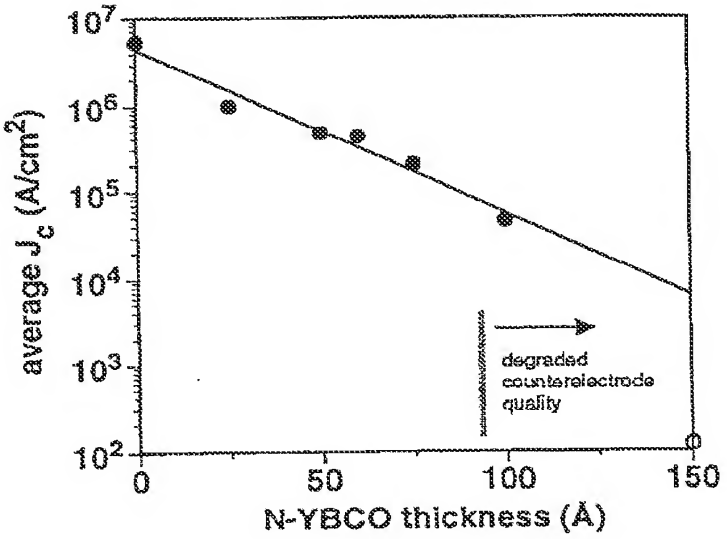

Figure 5. Plot of the average critical current density vs. N-YBCO thickness for 25 chips at 4.2 K. The line is a fit to $J_c = \exp(-L/\xi_n)$ for barrier thicknesses, L, less than or equal to 100 Å (solid points), and $\xi_n = 23$ Å is the effective normal metal coherence length.

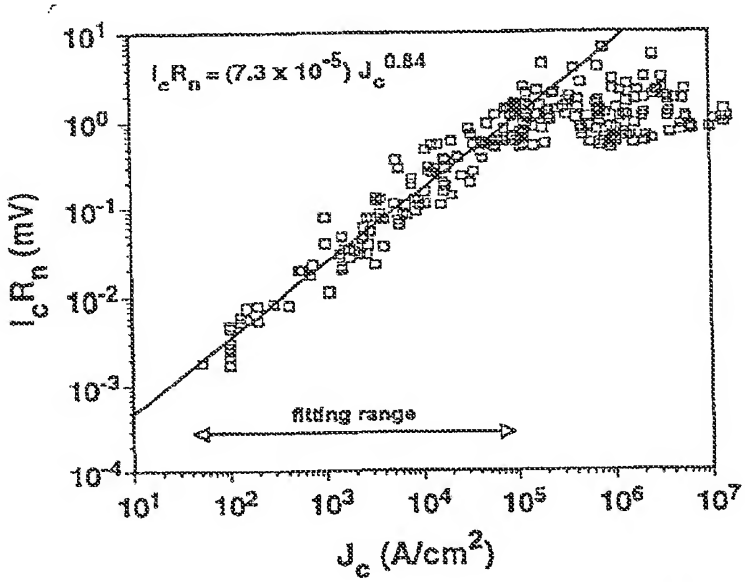

Figure 6. A plot of I_cR_n vs J_c for N-YBCO and ion-damage barrier devices on 33 chips at 4.2 K. The line is a fit to the data for $J_c < 10^5$ A/cm^2, indicating that I_cR_n scales as $J_c^{0.84}$ in this range.

ECS'93 and Spring MRS '93

Edge Cleaning Optimization and Ion-Damaged Barrier Weak Links

- Basic edge cutting and cleaning process:

1) Ion mill at 60° angle to produce tapered YBCO edge.
2) "Quasi-in-situ" transfer inside N_2-purged load-lock.
3) Normal incidence, low E ion clean.
4) Heat in O_2 for YBCO counterelec. growth.

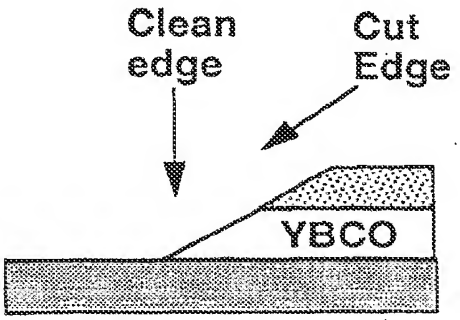

- Looking in the limit of zero barrier thickness, where the YBCO counterelectrode is deposited directly on the ion-milled base electrode edge.

- We have examined the dependence of the edge junction electrical properties on the edge cutting and cleaning parameters in this limit of "no barrier" in order to:

1) Optimize the cleaning procedure to obtain the cleanest possible YBCO-normal metal interface in weak links using deposited normal metals.
2) Investigate whether high quality, controllable weak links could be produced using an ion-damaged YBCO surface layer as a "normal metal"

Edge-Geometry, All-YBCO Weak Links with Ion-Damaged Barrier Layers

- YBCO edge produced by Ar-ion milling at 500 eV, and cleaned in-situ at 50 eV.
- T = 77 K; Device size is 3 μm x 0.46 μm

$J_c = 5.3 \times 10^4$ A/cm^2

$I_cR_n = 153$ μV (1.3 mV - 4.2K)

$R_nA = 2.9 \times 10^{-9}$ Ω-cm^2

(Ic=0.73mA, Rn=0.21Ω)

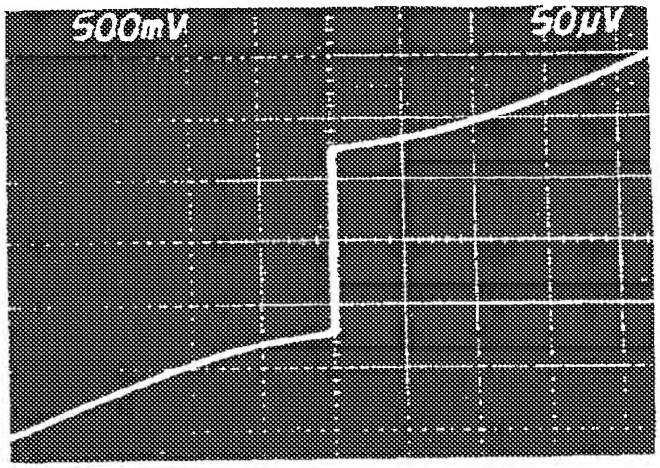

0.5 mA/div.

50 μV/div.

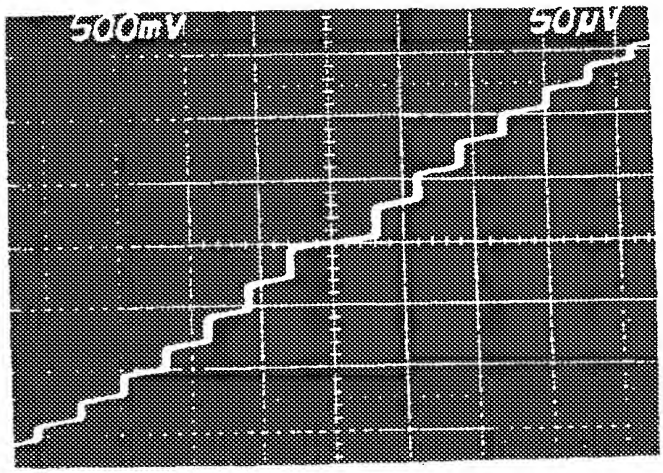

ac Josephson effect at 14.4 GHz

Step amplitudes vs RF field qualitatively consistent with theory.

device - 719921.2#7

JPL

Dependence on Edge Cleaning Parameters

- Examine J_c, I_cR_n, and R_nA as a function of Ar ion cleaning energy following 500 eV Ar edge mill:

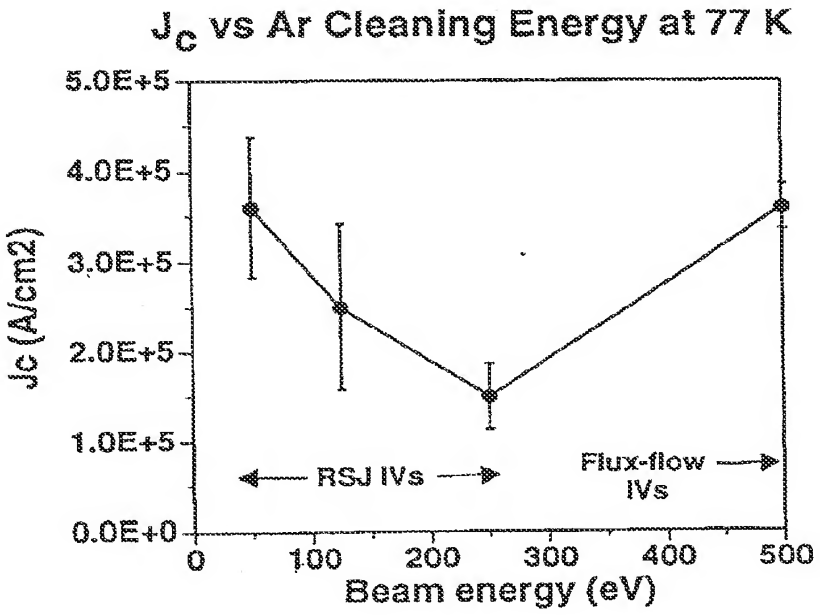

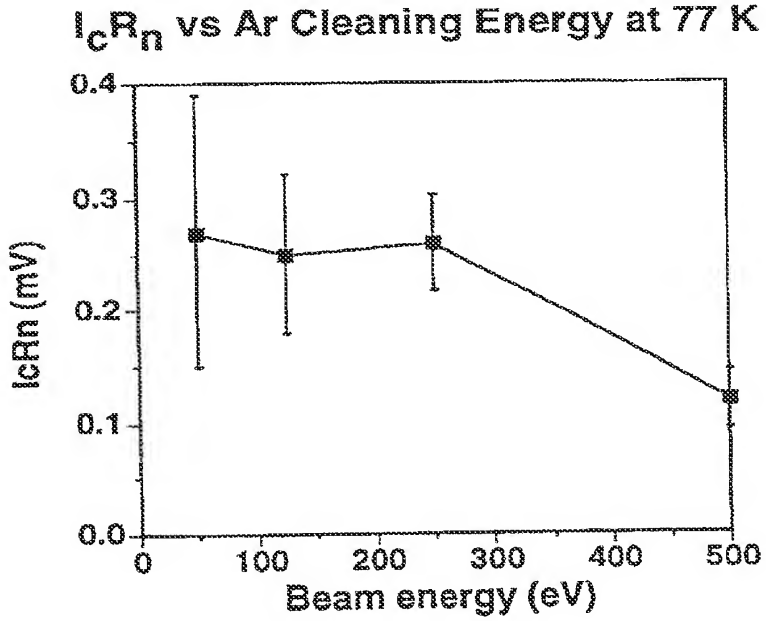

For 500 eV Ar edge cutting, 50 eV Ar cleaning gives best overall results

JPL

YBCO Edge Cleaning Results

- For 500 V Ar milling and 50 V cleaning at 4.2K:
  - Ave. $J_c = 5.5 \times 10^6$ A/cm^2 $\pm 4.7 \times 10^6$ A/cm^2
  - Ave. $R_nA = 5.4 \times 10^{-10}$ Ω-cm^2 $\pm 6.4 \times 10^{-10}$ Ω-cm^2
  - Ave. $I_cR_n = 1.03$ mV $\pm .24$ mV*

  *Note that I_cR_n may be limited by self-shielding effects in these very high J_c devices.

- We have also tried:
  1) Xenon cleaning --> Xe has ≈ 1/3 the range of Ar resulting in shallower surface damage - No significant difference seen.
  2) Eliminating the ion cleaning step - No significant difference seen.
  3) Varying the edge cutting energy - Lowering edge milling energy to 250 eV produced no real improvement.

JPL

Edge Cleaning Studies - Conclusions

- **Ion-Damaged Barrier Weak Link Fabrication:**
  - Excellent quality IVs at 77K ... may be useful for some applications.
  - However, this approach does have drawbacks:
    - » J_c is not controllable over wide range (advantage?)
    - » Device J_c is approaching electrode J_c --> can have problems with electrode transitions.
    - » R_nA products are small $\approx 5 \times 10^{-10}$ Ω-cm^2 --> need 0.1 μm lithography for 5 Ω devices.

- **Edge Cleaning Optimization:**
  - Process produces very clean edges with high J_c (5.5×10^6 A/cm^2) and low R_nA (5×10^{-10} Ω-cm^2) at 4.2K.
  - Measured I_cR_n products at 4.2K are $\approx$ 1mV. (limited by self-shielding effects?)
  - Futher optimization should be possible.